Orientation and Kinematic History of Faults, Veins and Sedimentary Intrusions in the AND-2A Sedimentary Rock Core, Southern McMurdo Sound, Antarctica

Senior Thesis

Submitted in partial fulfillment of the requirements for the

Bachelor of Science Degree

At The Ohio State University

By

David Michael Saddler

The Ohio State University

2010

Approved by

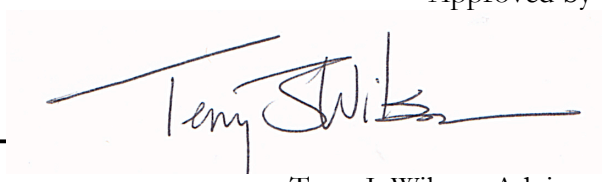

Terry J. Wilson, Advisor
School of Earth Sciences

Abstract:

The Southern McMurdo Sound (SMS) project recovered 1138 m of mainly Neogene rock core from the Victoria Land Basin of Antarctica, which is located in the westernmost branch of the Ross Sea rift system. Approximately 1008 natural fractures occur in the core including faults, veins, brecciated zones and sedimentary intrusions. This study contributed to the process of orientation of the core, and structures within it, to *in* situ coordinates by completing digital 'stitching' of core into intact core intervals. The attitudes of oriented structures were plotted on graphical stereonets to identify any consistently oriented sets of faults, veins and sedimentary intrusions. Twenty-one core intervals were analyzed and preliminary results indicate the orientation of the fault sets changes with depth from a dominant northwest trend downward to a dominantly northeast orientation. Change in fault orientation occurs at a regional marker reflector at 922.38mbsf, dated to ~19Ma. The northeast fault orientation observed in the older sedimentary rocks of the SMS core has also been observed in the Cape Roberts core to the north and for mapped, onshore faults. This provides evidence for transtensional rifting along the Transantarctic Mountain Front rift boundary in the Oligocene and Early Miocene.

Acknowledgments:

Special thanks to my advisor, Dr. Terry Wilson. Her support, guidance and vast knowledge helped to guide me through this very interesting study. She has made my research experience very informative as well as fun, and for that I thank her.

Many thanks also go to Cristina Millan and my other officemates Lauren, Stephanie, Jamey, Bill and Zach, who were also a great help throughout this entire process. Their sound advice on software programs, figures and technical support are greatly appreciated.

I would like to dedicate this thesis to my parents, Molly and Steve. Their continued support throughout my time at Ohio State has made all of this possible. No words can describe how thankful and truly blessed I am for the opportunities they have provided me.

Table of Contents

Abstract ..... **i**

Acknowledgment ..... **ii**

Introduction **1**

ANDRILL Project 1

Study Objectives 1

Geologic Setting **2**

Fractures in SMS Core **5**

Natural Fractures 5

Faults 5

Veins 5

Sedimentary Intrusions 6

Induced Fractures 6

Methods **8**

Core Logging 8

Core Orientation 9

Analysis of Natural Fracture Geometry 10

Results **13**

Discussion **16**

Conclusions **20**

References **21**

Introduction:

ANDRILL Project

ANDRILL is a multinational organization aimed at recovering a stratigraphic record from the Antarctic margins through the process of drilling rock cores. The Southern McMurdo Sound (SMS) drilling project aims at reconstructing the tectonic and climatic history of the Ross Sea region to better understand Antarctica's role on a global level. In 2007 the SMS project obtained 1138m of sedimentary rock core from McMurdo Sound in the southwestern corner of the Ross Sea. The main goal of paleoclimate studies on the SMS core is to map and construct a Neogene and younger ice volume and sea-level record for the Antarctic margin, from a location proximal to the ice sheet (Harwood et al., 2005). Tectonically the overall goal is to establish a Neogene subsidence history and structural history for the Victoria Land Basin, dating the episodes of proposed orthogonal and transtensional rifting in the western Ross Sea (Harwood et al., 2005).

Study Objectives

This project is part of a regional study of the structure of the Transantarctic Mountains Front fault zone and the offshore Terror Rift in the western Ross Sea. Structural data from the SMS core provides information about Neogene and younger deformation along the western side of the Victoria Land Basin. The overall goal of this project is to map the orientation of natural fractures in sedimentary rocks of the AND_2A core (ANDRILL's official name for the SMS core) using stereographic analysis. This result contributes to developing a regional fault history based on fault stratigraphy, cross-cutting relationships, and the age of sedimentary rock units. This study determined whether orientation patterns of natural fractures in the SMS core are consistent with faulting along the Transantarctic Mountain Front boundary of the Victoria Land Basin to the west or faulting of the young Terror Rift to the east in the Ross Sea.

Geologic Setting:

The AND-2A sedimentary rock core is located in southern McMurdo Sound in the western Ross Sea, Antarctica (Figure 1). The sedimentary rocks cored were deposited in the Victoria Land Basin (VLB), an elongated north-south trending extensional basin. The Victoria Land Basin is a structural half-graben approximately 350 km long (Florindo et al, 2009). The VLB is bordered by the Transantarctic Mountain Front (TMF) fault zone along the coast to the west. The younger Terror Rift developed within the VLB. Fault and flexure-related subsidence associated with rifting and volcanic loading has provided Paleogene to Quaternary stratigraphic accommodation space adjacent to the rising Transantarctic Mountains. The combination of high sediment supply from glacial activity in the Transantarctic Mountains paired with accommodation space from thermal subsidence and rifting have made the Victoria Land Basin a great repository of earth history for the past c. 50 m.y. (Florindo et al, 2009).

The sedimentary basins in the Ross Sea, including the VLB, have been formed by crustal extension since Gondwana breakup (Fitzgerald, 2002). These basins are part of a larger rift system known as the West Antarctic rift system (WARS). Basin formation began with development of a rift zone associated with Jurassic magmatism, subsidence and possible strike-slip motion. Between c. 105 and 85 Ma the phase of greatest extension between East and West Antarctica occurred in the Ross Sea. Total extension is poorly constrained. However, simple one-layer stretching models suggest c. 400km of extension (Fitzgerald, 2002). This extension in the horizontal direction resulted in crustal thinning in the vertical direction. Total extension paired with the high sediment supply has provided up to 10km of sediment in the Victoria Land Basin and other basins located in the Ross Sea (Naish et al., 2006).

The Transantarctic Mountains run along the western coast of the Victoria Land Basin with a length of over 4500 km and relief of more than 4000 m (Salvini et al., 1997). Regional basement is composed primarily of late Proterozoic-Cambrian metamorphic rocks and Cambrian-Ordovician granitiods (Fitzgerald, 2002.) Basement rocks were deformed during the Ross Orogeny that preceded

and accompanied granitiod intrusions. The boundary between the VLB and the Transantarctic Mountains is marked by a zone of normal faulting, known as the Transantarctic Mountain Front fault zone (TMF). The TMF zone typically extends c. 20 to 30 km inland from the coast, and normal faulting in this zone accommodated 2 to 5 km of displacement between the TMF and the down-dropped VLB (Fitzgerald, 2002). The trend of the TMF to the west of the SMS site has been demonstrated to be about N20°W from subsurface seismic data (Pekar et al., 2009; Sunwall et al., 2009). In the Victoria Land Basin a thick, east-dipping sedimentary package has filled the accommodation space created by normal faulting (Figure 2). Most displacement on the TMF fault zone is interpreted to have occurred in the latest Eocene-Oligocene time period, during syntectonic deposition of sediments in the Victoria Land Basin (Wilson and Paulsen, 2001).

The Terror Rift in the Ross Sea to the east of the SMS site is superimposed on the Victoria Land Basin. Faults of the Terror Rift reach the seafloor, indicating that it is the youngest faulting in the rift system (Naish et al., 2006). Post-early Oligocene extension has only occurred within the narrow Terror Rift zone within the Victoria Land Basin (Cooper and Davey, 1985). Neogene extension in the Terror Rift is associated with igneous intrusions around Ross Island (Cooper et al, 1987).

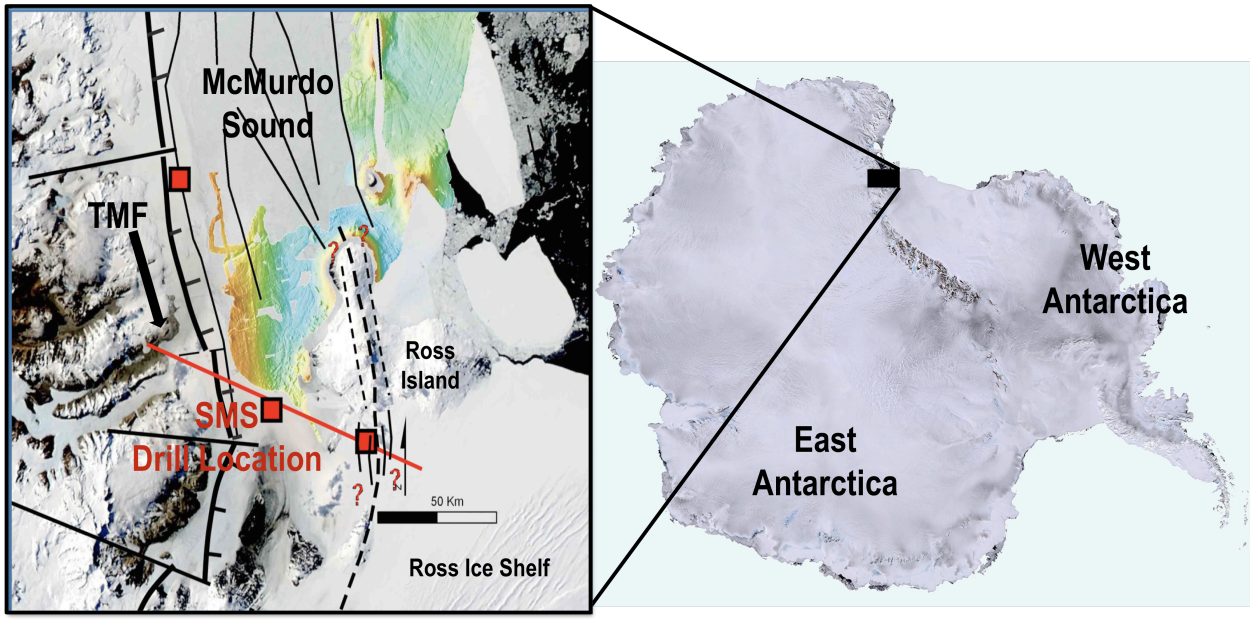

Figure 1. The SMS drill location is located in the southwestern portion of McMurdo Sound in the Ross Sea, Antarctica. Geographically the site is located between the Transantarctic Mountains to the west, Ross Island to the east and the Ross Ice Shelf to the south (Wilson, unpublished).

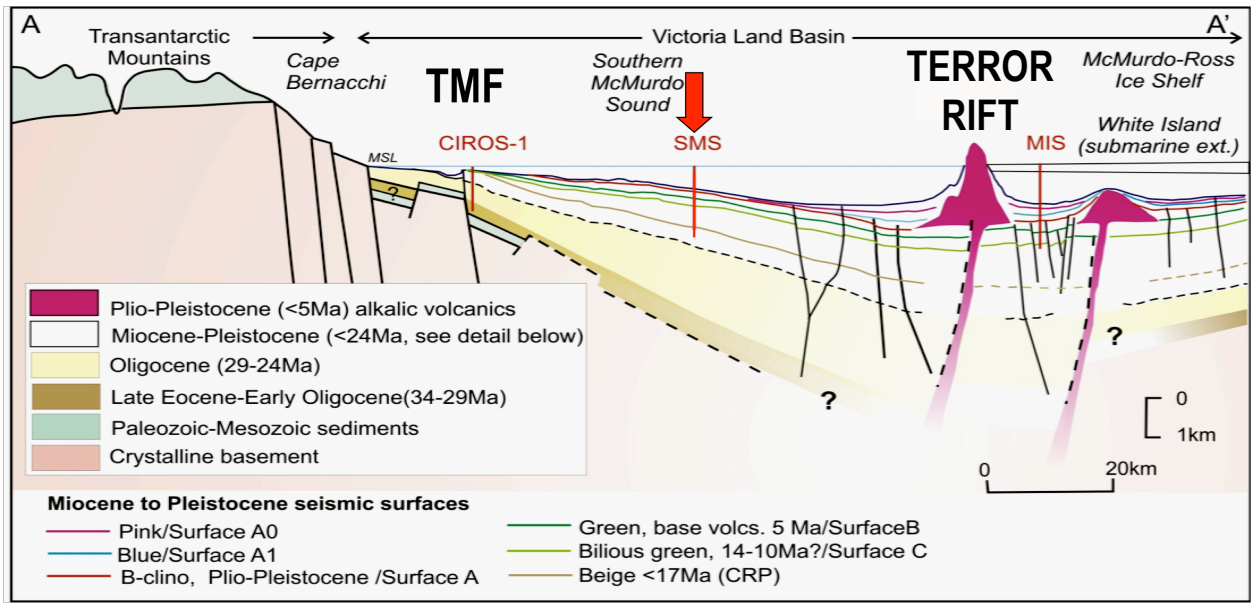

Figure 2. The SMS project drilled into the Victoria Land Basin, a thick east-dipping sedimentary basin. The basin sits to the east of normal faulting along the Transantarctic Mountain Front (TMF) fault zone and is superimposed by faulting of the young Terror Rift to the east of the drill site (modified from Florindo et al., 2009).

Fractures in SMS Core:

Natural Fractures:

A natural fracture is defined as any cored fracture that existed in a volume of rock prior to initiation of drilling (Kulander et al., 1990). Natural fractures are identified based on their geometry and characteristics, such as truncation/offset of bedding, mineralization or brecciation (Paulsen et al., 2008). Three types of natural fractures were analyzed in the SMS core: faults, veins and sedimentary intrusions (Figure 3).

Faults

Faults are fractures on which slip develops primarily by brittle deformation processes (van der Pluijm and Marshak, 2004). Faults exhibit either normal shear sense or reverse shear sense. Normal faulting occurs when the block above the fault, or the hanging-wall, moves down relative to the block below the fault surface, or footwall. Normal faulting results in overall extension horizontally. Reverse faulting is the opposite. In a reverse fault the footwall moves upward relative to the hanging-wall. This results in overall contraction or shortening of the beds in the horizontal direction. Normal faulting is dominant in the AND-2A core, however a few reverse faults are found.

Veins

Veins are nearly planar fractures filled with mineral crystals that precipitated from solution (van der Pluijm and Marshak, 2004). Typically vein fill exhibits either blocky or fibrous crystals. In blocky veins, the crystals of vein fill are roughly equant. Blocky vein fill means that the vein filled a preexisting cavity in the rock (van der Pluijm and Marshak, 2004). In fibrous veins, the crystals are long relative to their width. This type of vein fill indicates opening of the fractures in the rock occurred at the same time as mineral precipitation of the vein material (van der Pluijm and Marshak, 2004). The presence of veins indicates abundant fluids, substantial pore pressures, and a strong role of fluids in deformation of the strata (Paulsen et al., 2008). In the AND-2A rock core fibrous veins are more abundant. Veins are

typically steeply dipping, >75°. Veins that are associated with faulting typically show a lower dip angle, between 50° and 70°.

Sedimentary Intrusions

Sedimentary intrusions, or clastic dikes, are forcefully injected sedimentary structures associated with fluid-sediment movement as a response to loading and/or tectonic stresses (Collinson, 1994). Intrusions are most commonly from below and form due to pressure from overlying beds. Over-pressuring must be sufficient enough to overcome any strength increase due to cementation or compaction that occurred during the burial history. However, in all cases, the liquefied sand or mud must have been buried by less permeable cohesive sediment (Collinson, 1994). Many closed fractures filled with granular material occur throughout the AND-2A core and appear to be sedimentary intrusions. Some intrusions clearly originate from sedimentary beds below and contain material derived from them; others are filled with clastic material of unknown origin (Paulsen et al., 2008).

Induced Fractures:

Induced fractures are fractures that form during drilling (i.e. in the rock around the drill bit), coring (i.e. on entry or in the core barrel), or subsequent handling of the core (Kulander et al., 1990). Petal, petal-centerline and core edge fractures are the most abundant in the AND-2A core (Paulsen et al., 2008). They are defined by very steep dips that die out down core or exit along the core edge. Fractographic features, including arrest lines and fine hackle plumes, demonstrate propagation of these fractures inward and downward along the core axis (Paulsen et al., 2008). Induced fractures are significant because they provide the orientation of the present day *in situ* stress field for the region. However, induced fractures are not the topic of this study.

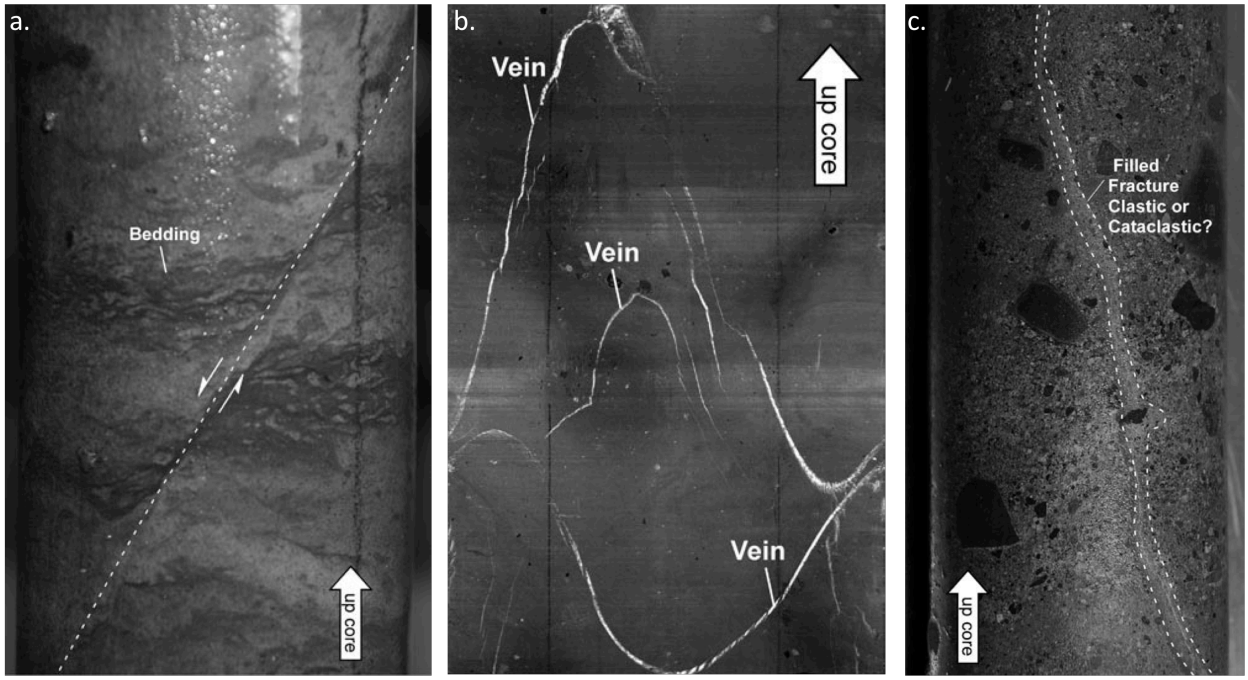

Figure 3. (a.) Fault showing normal offset of bedding in the AND-2A core. (b). Calcite vein fill as seen in an 'unrolled' whole-core scan of the AND-2A core. (c.) Fracture filled with either clastic or cataclastic material in the AND-2A core (Paulsen et al., 2008)

Methods:

Core Logging

The SMS project drilled core in three different diameters. 'PQ' core has a diameter of 83mm, 'HQ' has a diameter of 61mm and 'NQ' has a diameter of 45mm. "Intact intervals" are continuous lengths of core where no internal relative rotation has occurred (Figure 4). The boundaries of these intact intervals are either ends of core runs where core could not be fitted back together or induced fractures in the core that experienced spinning during the coring process. Intact intervals were mapped during core logging at the drill site (Paulsen et al., 2008). In the PQ core, 44% of core runs could be fitted together, with a maximum intact interval of 12.91 m in length. In the HQ core, 66% of the core runs could be fitted at their ends, and intact core intervals up to 75.62 m-long were found. In the NQ core, 54% of the core runs could be fitted at their ends, with a maximum core interval length of 16.87 m (Paulsen et al, 2008).

Core was extracted from the ground in metal machined core splits. An additional split was machined with slots along its axis separated by 180 degrees. The core was scribed with a red line and a blue line in each of the two machined slots (Figure 5). The red line was treated as an 'arbitrary north' and all fracture orientation measurements were made with respect to the red line. In some cases, the red line was found to be unreliable. In these cases, measurements were made with respect to the blue scribe line.

All natural and induced fractures were recorded at the drill site, and depth, dip azimuth and dip angle were recorded on log sheets. The top and bottom depths of each fracture were measured in mbsf. Dip direction and angle were measured using templates created for each diameter core (Figure 6). Templates were placed over top of the core and dip direction was measured with respect to the red scribe line. Using a dip angle template, a best fit curve was found for each fracture.

Core Orientation

Core was cut into lengths of one meter. Whole-round core segments were imaged using a digital scanner that recorded the exterior surface of the core as it revolved on rollers, producing an 'unrolled' image of the circumference of the core segment. Some highly fractured segments could not be scanned because they would have fallen apart during rolling in the scanning process. Core images were obtained of 73% of PQ core (between 0-229.24 mbsf), 88% of HQ core (between 229.4 and 1011.87 mbsf), and 97% of NQ core (between 1011.87 and 1138.54 mbsf) (Paulsen et al, 2008). Each core scan file was named in meters below sea floor of the top of the core segment.

I imported and manipulated whole core images in Adobe Photoshop to better define the red scribe line. I then loaded images into DMT CoreBase® software to be digitally 'stitched' together into intact intervals of core. CoreBase® allows each individually scanned segment to be shifted up and down as well as rotated clockwise and counterclockwise. The images were put back together based on matching the red scribe line that served as the arbitrary 'north' direction. Fit angles between core runs were accounted for according to the depths and rotational angles recorded on the logging sheets. Errors in scribing were corrected for during the digital stitching process. Errors in the original core scribing or scanning were corrected by matching natural features such as fracture planes, large clasts or veins. In these cases, the 'misfit angles' of these corrections between core images were recorded. An image of each interval was exported from CoreBase® after it was digitally stitched together.

The images of each stitched interval as well as a spreadsheet record of every shift, rotation, fit and misfit was sent to a colleague at the University of Utah. The digital core images were compared with imaging from a borehole televiewer (BHTV). The BHTV is a magnetically oriented acoustic sounding device that is lowered into the hole after the coring process. It records an image of the borehole wall including features such as fracture and bedding planes, as well as large clasts in diamictite lithologies. The image produced from the BHTV was compared with the stitched core image to find matching

features (Figure 7). The matching features were used to calculate an average rotation angle for each intact interval to restore the red scribe line on the core to true geographic north given by the BHTV image. I applied this rotation angle to the orientations of structures recorded on the log sheets to place fractures, veins and sedimentary intrusions back to their true north orientation.

Analysis of Natural Fracture Geometry

This study analyzed the *in situ* orientation data for all natural fractures in oriented SMS core using 'stereonet' software provided online by R. Allmendinger (http://www.geo.cornell.edu/geology/faculty/RWA/programs.html). This plotting program was used to plot strike, dip and dip direction for each natural fracture obtained from the logging sheets. Fractures in each intact interval were divided into four structural types: faults, veins, sedimentary intrusions (clastic dikes) and 'unknown' types. All four types were plotted for each intact interval. Plots for each fracture type were compared within single intervals. Plots were also compared between intact intervals to view down core trends of fractures. Comparison between plots of definite fracture types and 'unknown' types were made. If 'unknown' fractures matched the trends of 'definites' they were flagged and moved to the definite plots. This was only done where additional data from notes and sketches from the original logging sheets provided substantiating evidence. Finally, kinematic analysis of fractures in intact intervals was completed. Faults were separated into normal and reverse categories and plotted separately to view trends. Veins were also divided into several categories including opening-mode, fault-related and folded types. They were also plotted separately to view any differences in orientation. Changes in orientation paired with age constraints of rock units can provide a kinematic history and linked changes in stress field orientation over time.

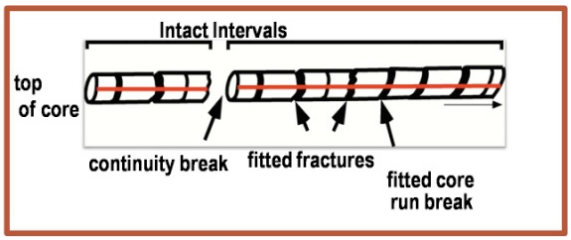

Figure 4. “Intact intervals” boundaries are either ends of core runs that could not be fit together, or drilling induced fractures that spun during the coring process (Paulsen and Wilson, 1998).

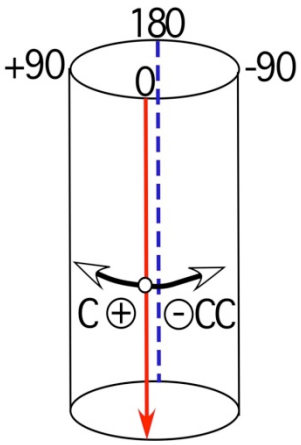

Figure 5. Core was scribed with a red line and a blue line separated by 180 degrees. The red line was treated as an ‘arbitrary north’ from which measurements were made (Paulsen et al., 2008).

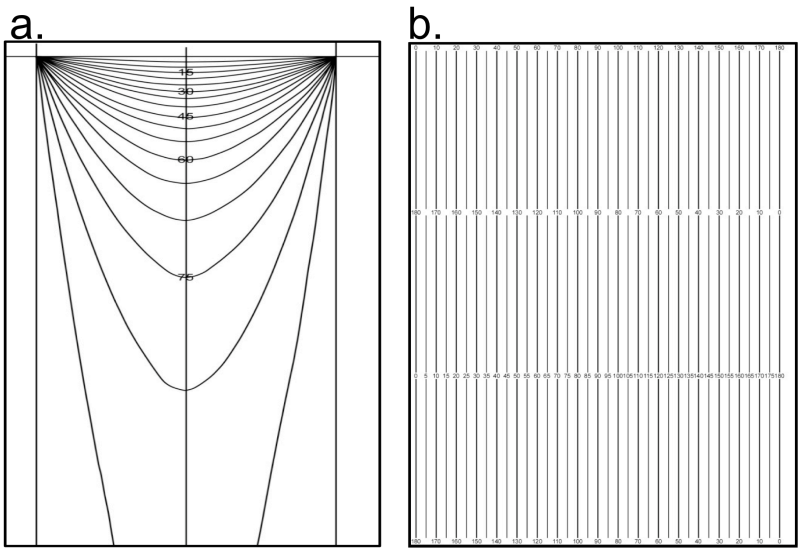

Figure 6. (a.) Template was used to measure a best fit dip direction and angle. (b.) Template was used to measure a best fit dip azimuth with respect to the red scribe line (Wilson, unpublished).

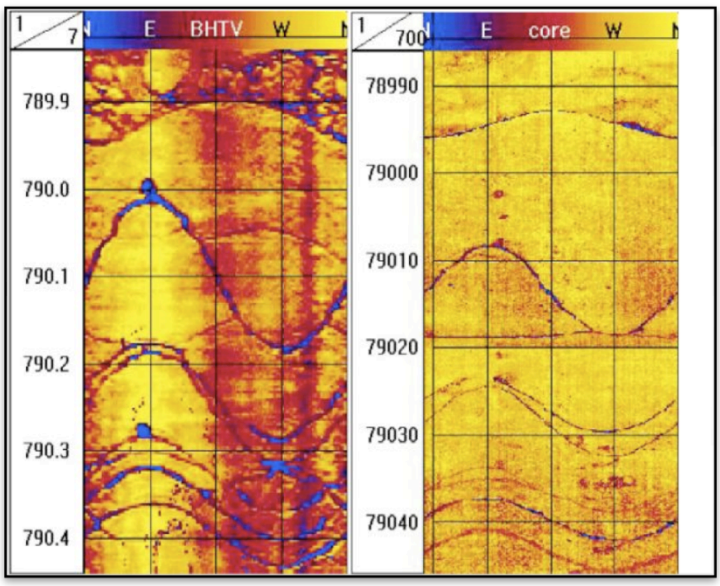

Figure 7. Fractures from the digitally stitched core image can be matched to fractures found from the BHTV imaging of similar depth. BHTV sinusoids have higher amplitudes due to a larger image diameter (Jarrard et al., 2001)

Results:

For this study, twenty-one intervals totaling 352.55m of SMS core were digitally stitched at the Ohio State University and successfully oriented at the University of Utah using the feature matching process. A total of 90 veins, 91 faults and 2 clastic dikes were restored to their *in situ* orientations. 168 fractures are unclassified but could potentially be moved to one of the three definite structural types after further analysis of orientation and examination of log sheets, photographs and core scans.

Table A presents the structural types present in each intact interval of core. Appendix A presents stereoplots of veins, faults and clastic dikes for each intact interval. Appendix B presents the tables from which each plot was made. Below, orientation patterns demonstrated by these plots are summarized.

Interval 398.05 contains one of the two clastic dikes. This clastic dike has a northeast orientation with a northward dip. Interval 407.61 consists only of faults. Fault orientations and dips are scattered and no consistent trend is observed. Interval 497.26 also consists of only faults, however there are many more unidentified natural fractures. Faults are steeply dipping and have a consistent northeast trend. Interval 527.41 only contains veins with a few unidentified fractures. Vein orientation is scattered but all exhibit a steep dip. Interval 570.52 contains mostly faults with one vein present. Faults show a consistent northwest trend with consistent, moderate, southwest dips. The vein exhibits a north-south orientation with a steep dip. Interval 582.4 contains faults with many unidentified fractures. Faults show a northwest trend with one outlier trending northeast. Interval 647.53 consists only of faults. Faults show a northwest trend with some scatter and one fault trending north-south. All faults dip to the northeast. Interval 666 contains mostly faults with two veins present. Faults show a northeast trend with one northwest outlier. Both veins have a northwest trend but vary in dip angle. Intervals 753.92 and 778.57 contain no definite fracture types. Interval 837.63 consists of faults with many unidentified fractures. Faults have a west-northwest trend with one fault trending north-south. The faults have a

consistent southwest dip of about 70°. Interval 852.01 is dominated by veins but also contains two faults and the deepest clastic dike seen in the core. Veins exhibit a very strong northwest trend with consistent subvertical dips. Faults are also steeply dipping and show north-south and east-northeast orientations. The clastic dike also shows a northwest trend similar to the veins in this intact interval. Interval 880.98 contains no definite fracture types. Interval 895.43 is dominated by veins with two faults and no unclassified fractures. Veins show a scattered orientation with no trend visible. Faults are oriented northeast and are a conjugate set. Interval 898.11 contains the most natural fractures of any intact interval. Fracture type is dominated by faults with numerous veins also present. Faults form conjugate sets with a northeast trend. The majority of faults exhibit an eastward dip while the remaining faults have an opposing westward dip direction. Veins also have a northeast orientation and dominantly steep dips. Interval 916.16 consists of faults and an equal amount of unclassified fractures. Fault orientation is again northeast. Dips are to the east with one fault exhibiting a conjugate westward dip as seen up core. Interval 926.32 contains the highest concentration of veins of all intact intervals. Veins are steeply dipping and trend north-northwest. A few additional faults have scattered orientation. Interval 971.72 contains only faults. Fault orientation is scattered and no consistent trend is observable. Interval 1036.80 contains one vein with an east-northeast orientation. Interval 1068.84 contains one vein and one fault. The fault has a northwest orientation whereas the vein exhibits a northeast trend. Interval 1100.29 is dominated by veins. Veins trend north-northeast and are dominantly steep.

Table A:

Interval Depths		Number of Veins	Number of Faults	Number of Clastic Dikes	Number of Unidentified Fractures
398.05-407.24		NONE	NONE	1	10
407.61-425.7		NONE	6	NONE	2
497.26-527.41		NONE	3	NONE	18
527.41-546.35		4	NONE	NONE	3
570.52-582.2		1	4	NONE	5
582.4-587.1		NONE	4	NONE	7
647.53-666		NONE	7	NONE	13
666-701.68		2	5	NONE	14
753.92-761.34		NONE	NONE	NONE	5
778.57-784.31		NONE	NONE	NONE	2
837.63-852.01		NONE	7	NONE	13
852.01-875.60		8	2	1	29
880.98-886.37		NONE	NONE	NONE	20
895.43-897.44		8	2	NONE	NONE
898.11-919.16		13	33	NONE	2
916.16-926.32		NONE	8	NONE	9
926.32-971.72		31	NONE	NONE	13
971.72-1001.94		NONE	9	NONE	NONE
1036.80-1049.13		1	NONE	NONE	NONE
1068.84-1082.92		1	1	NONE	2
1100.29-1117.17		21	NONE	NONE	1
Total		90	91	2	168

Discussion:

The orientation patterns of natural fractures documented in this study indicate the orientation of fault sets changes with depth from a dominant northwest trend downward to a dominantly northeast orientation. The change in orientation occurs near a regional seismic reflector at a depth of 922.38mbsf, dated to ~19Ma (Figure 8). Faults above this regional marker showed a strong northwest trend with dip angles ranging from 48 to 79 degrees. All faults above 898.11 mbsf yield an average orientation of N19°W, 70°S. All faults below 898.11 mbsf have an average orientation of N30°E, 69°E. Veins show a more consistent northerly orientation throughout the core. Veins above 898.11 mbsf show an average orientation of N6°W, 80°W. Below 898.11 mbsf the average orientation of veins is N9°W, 81°E (Figure 9).

Lithology seems to have no influence on fault orientation. Therefore, I suggest that a change in stress field orientation is responsible for the change in fault orientation seen at the 19Ma regional marker bed.

Fault orientation above the 19Ma regional marker is consistent with attitudes mapped along the Transantarctic Mountain Front fault zone. The TMF shows an average orientation of N20°W from seismic data, which is nearly identical to the N19°W average orientation found for fractures in the SMS core. Given this parallel geometry, it is possible that the northwest-trending faults in the core are related to the TMF fault zone. If so, the fault zone has been active for the past 19 million years.

Faults below the 19Ma regional marker show a strong northeast trend of N30°E. This northeast orientation is oblique to the TMF fault zone, but is very similar to fault trends found in the Cape Roberts Project (CRP) which obtained 939.42m of sedimentary rock core to the north of the SMS drill location (Bucker et al., 2001). CRP drilled primarily Oligocene sedimentary rocks, the same age as those found in the bottom of the SMS core. At Cape Roberts, faults in the core have similar orientation to both onshore and offshore faults mapped along the TMF in the region (Wilson, 1995; Hamilton et al., 2001). Most

significantly, a north-northeast-striking normal-displacement fault set is dominant in the core (Wilson and Paulsen, 2001). This orientation coincides with the normal-displacement fault orientation seen in sedimentary rocks below 898mbsf in the SMS core. Since the rock units affected in the SMS core are Early Miocene-Late Oligocene in age, this regional deformation event must have occurred in Miocene and older times.

Vein orientation both above and below the 19Ma regional marker are fairly consistent. Both exhibit a relatively north-south strike, however veins have an average dip to the west above the marker and to the east below the marker. Further kinematic analysis to determine if the veins and faults formed at the same time, in response to the same stress regime, is required to interpret the significance of this result.

Natural fracture patterns in the SMS core support a regional >19Ma event that produced northeast faults in the Victoria Land Basin, which must have extended obliquely to the TMF. This oblique rifting along the TMF has been interpreted from onshore kinematics (Wilson, 1995), but the age of faulting is poorly constrained there. This study, together with CRP results and onshore mapping, provides evidence for transtensional rifting along the TMF rift boundary in the Oligocene and Early Miocene.

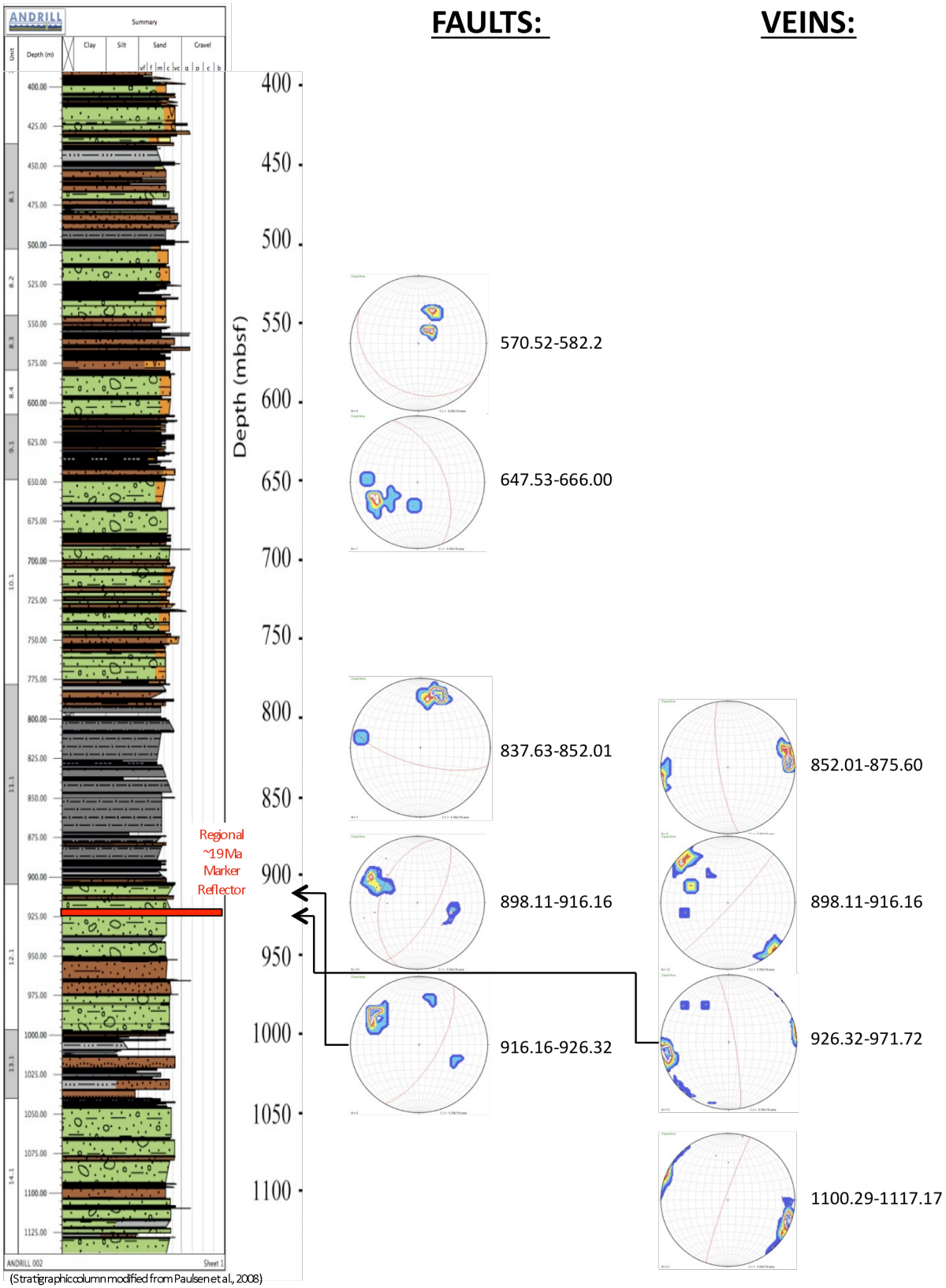

Figure 8. Stratigraphic column with lithological changes compared with average fault and vein orientations of different depths (mbsf). Regional marker reflector is marked in red.

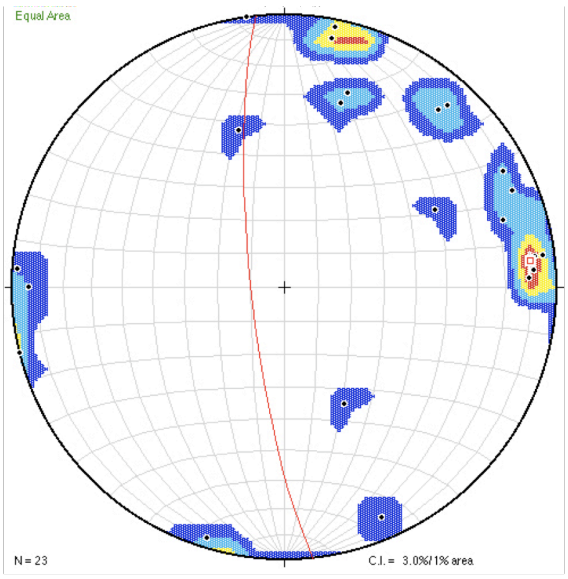

Veins above 898.11mbsf:
N6°W, 80°W

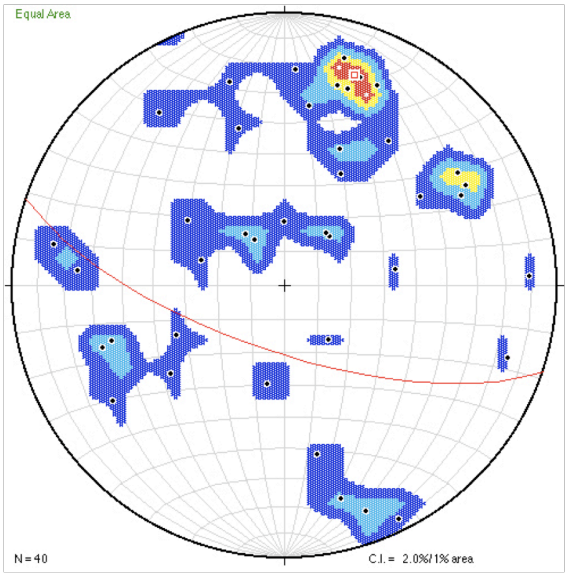

Faults above 898.11mbsf:
N74°W, 70°S

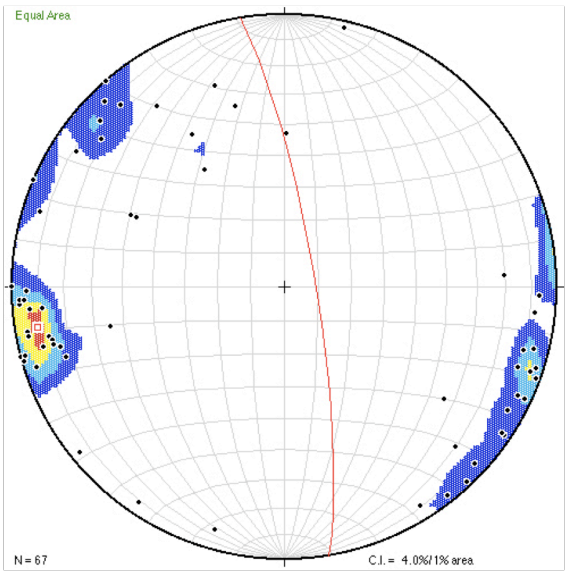

Veins below 898.11mbsf:
N9°W, 81°E

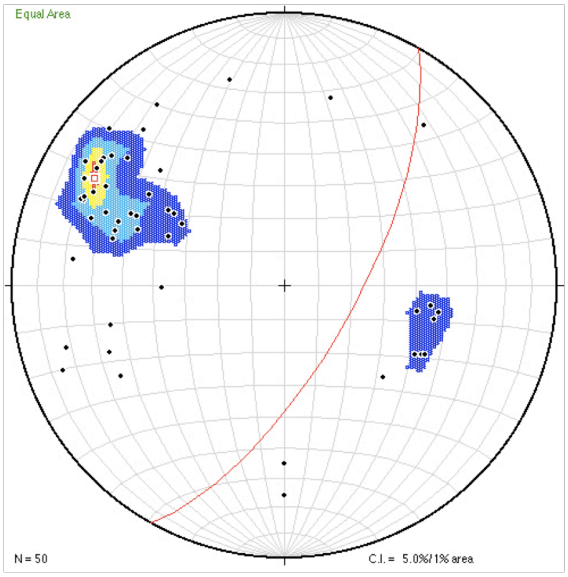

Faults below 898.11mbsf:
N30°E, 69°E

Figure 9. Average fault and vein orientations above and below 898.11mbsf. Veins show a consistent north-northwest trend while faults change from a west-northwest to northeast orientation down core.

Conclusions:

This study has shown that orientation of the fault sets in the SMS core changes with depth from a dominant northwest trend downward to a dominantly northeast orientation. Change in fault orientation occurs at a regional marker reflector at 922.38mbsf, dated to ~19Ma. The northwest orientation has a parallel geometry to the seismically mapped orientation of faults along the TMF fault zone. It is then possible that the faults are related to the TMF fault zone. If so, the fault zone has been active for the past 19 million years. The northeast orientation observed in the older sedimentary rocks of the SMS core has also been observed in the Cape Roberts coring project to the north and from mapped, onshore oblique faulting. This provides evidence for transtensional rifting along the Transantarctic Mountain Front rift boundary in the Oligocene and Early Miocene.

References:

Bucker, C.J., Jarrard, R.D., & Wonik, T. (2001). Downhole temperature, radiogenic heat production, and heat flow from the CRP-3 drillhole, Victoria Land Basin, Antarctica. *Terra Antarctica*, *8*(3), 151-159.

Collinson, J., 1994. Sedimentary Deformation Structures. In: Maltman, A. (ed.), *The geological deformation of sediments.* London, UK: Chapman and Hall, 1994.

Cooper, A.K., Davey F.J. (1985): Episodic rifting of the Phanerozoic rock of the Victoria Land Basin, western Ross Sea, Antarctica. *Science* 229: 1085-1087.

Cooper, A.K., Davey, F.J., Behrendt, J.C., 1987. Seismic stratigraphy and structure of the Victoria Land Basin, Western Ross Sea, Antarctica. In: Cooper, A.K. and Davey, F.J. (eds.), *The Antarctic Continental Margin:Geology and Geophysics of the Western Ross Sea.*CPCEMR, 5b, Houstin, Texas:27-77.

Fitzgerald, P. (2002). Tectonics and landscape evolution of the Antarctic plate since the breakup of Godwana, with emphasis on the West Antarctic Rift System and the Transantarctic Mountains. *Royal Society of New Zealand Bulletin*, *35*, 453-469.

Florindo, F., Harwood, D.M., Talarico, F., Levy, R.H., & and the ANDRILL-SMS Team . (2009). Background to the ANDRILL Southern McMurdo Sound project, Antarctica. *Terra Antarctica*, *15*(1), 13-20.

Hamilton, R.J., Luyendyk, B.P., & Sorlien, C.C. (2001). Cenozoic tectonics of the Cape Roberts rift basin and Transantarctic Mountain Front, southwestern Ross Sea, Antarctica. *Tectonics*, *20*(3), 325-342.

Harwood D.M., Florindo F., Levy R.H., Fielding C.R., Pekar S.F., Speece M.A. and the SMS Science Team , 2005. ANDRILL Southern McMurdo Sound Project Scientific Prospectus. ANDRILL Contribution No. 5. University of Nebraska-Lincoln, Lincoln, NE, 29 pp.

Jarrard, R.D., Paulsen, T.S., & Wilson, T.J. (2001). Orientation of the CRP-3 core, Victoria Land Basin, Antarctica. *Terra Antarctica*, *8*(3), 161-166

Kulander, B.R., Dean, S.L., & Ward, Jr., B.J. (1990). *Fractured Core Analysis: interpretation, logging, and use of natural and induced fractures in core*. Tulsa, OK: The American Association of Petroleum Geologists.

Naish T.R., Levy R.H., Powell R.D., and the MIS Science and Operations Team Members, 2006. *Scientific Logistics Implementation Plan for the ANDRILL McMurdo Ice Shelf Project.* ANDRILL Contribution 7. University of Nebraska-Lincoln, Lincoln-NE. 117pp.

Paulsen T., Millan C., Pierdominici S., Wilson T., Drew S. & the ANDRIL-SMS Science Team, 2008. Fracture Logging of the AND-2A Core, ANDRILL Southern McMurdo Sound Project, Antarctica. Terra Antarctica, 15(1), 69-76.

Paulsen, T.S., & Wilson, G.S. (1998). Orientation of the CRP-1 core. *Terra Antarctica*, *5*(3), 319-325.

Pekar, S. F., Speece, M. A., Sunwall, D., Wilson, G. S., Harwood, D. M., Florindo, F., and Tinto, K., 2009, Using new tools to explore undiscovered country: understanding the stratigraphic and tectonic history of greenhouse to icehouse worlds of offshore New Harbor, western Ross Sea, Antarctica: *First Antarctic Climate Symposium*, http://213.97.77.165/descargas/ANTARCTIC2009.rar, Abstract 3492.

Salvini, F., Brancolini, G., Busetti, M., Storti, F., & Mazzarini, F., Coren, F., (1997). Cenozoic geodynamics of the Ross Sea region, Antarctica: Crustal extension, intraplate strike-slip faulting, and tectonic inheritance. *Journal of Geophysical Research*, *102*(B11), 24,669-24,696.

Sunwall, D. A., Speece, M. A., Pekar, S. F., Wilson, G. S., and Tinto, K. J., 2009, An Over-Sea-Ice Seismic Reflection Survey: Offshore New Harbor, Antarctica: *Eos Trans. AGU*, 90(52), Fall Meet. Suppl., Abstract PP43A-1566.

van der Pluijm, B.A., & Marshak, S. (2004). *Earth Structure: an introduction to structural geology and tectonics*. New York City, NY: W. W. Norton and Company, Inc..

Wilson, T.J., & Paulsen, T.S. (2001). Fault and Fracture patterns in CRP-3 core, Victoria Land Basin, Antarctica. *Terra Antarctica*, *8*(3), 177-196.

Wilson, T.J. (1995). Cenozoic transtension along the Transantarctic Mountains-West Antarctic rift boundary, southern Victoria Land, Antarctica. *Tectonics*, *14*(2), 531-545.

Appendix A:

Depth: 398.05-407.24

VEINS	FAULTS	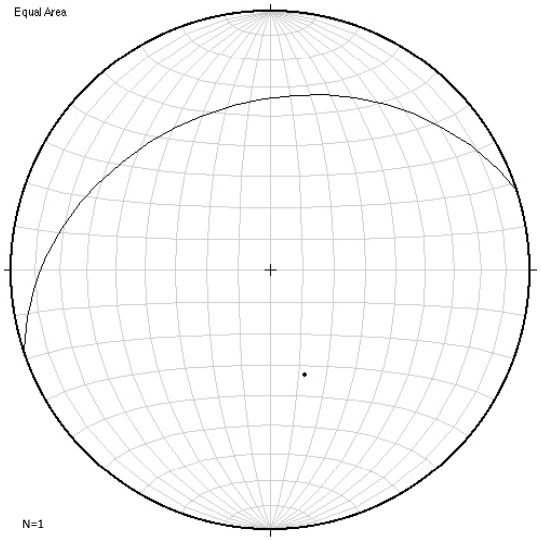 CLASTIC DIKES
		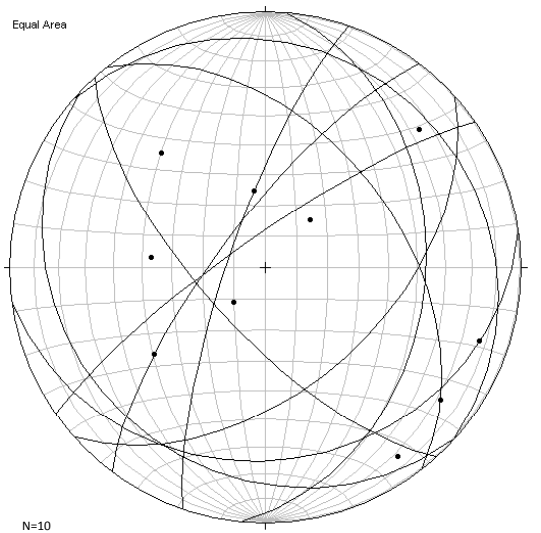 Unclassified Fractures

Appendix A:

Depth: 407.61-425.70

VEINS	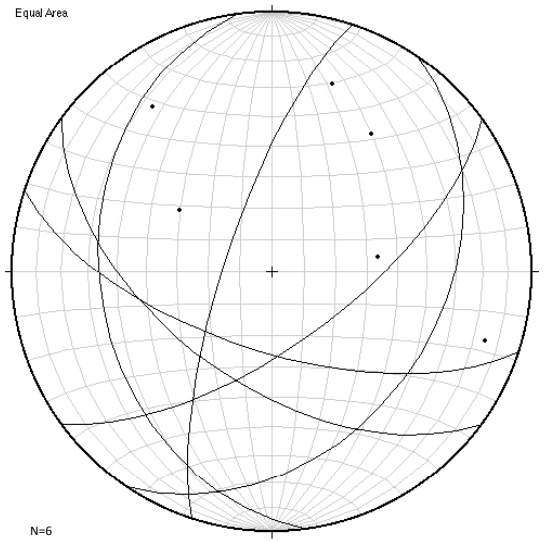 FAULTS	CLASTIC DIKES
		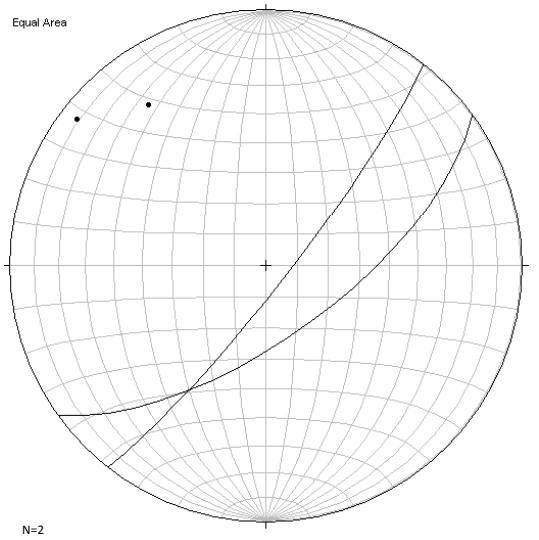 Unclassified Fractures

Appendix A:

Depth: 497.26-527.41

	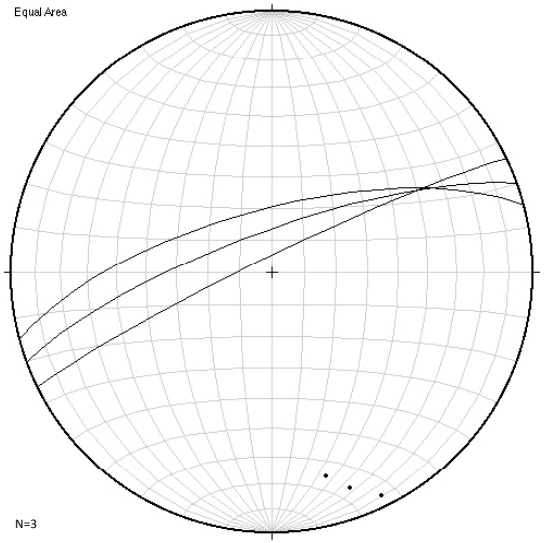	
VEINS	FAULTS	CLASTIC DIKES
	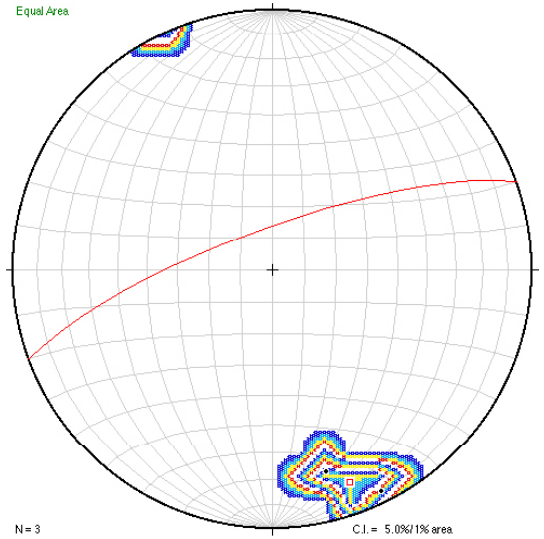	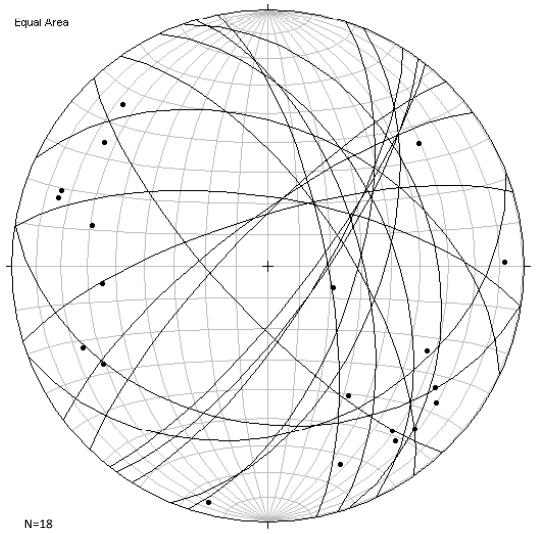
	Average Fault Orientation: N70°E, 77°N	Unclassified Fractures

Appendix A:

Depth: 527.41-546.35

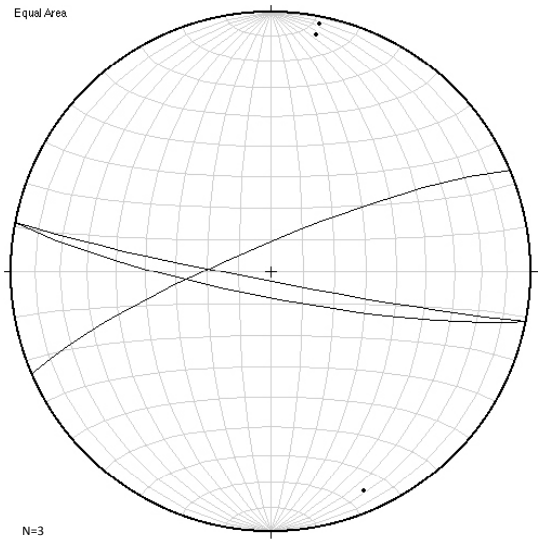

VEINS

FAULTS

CLASTIC DIKES

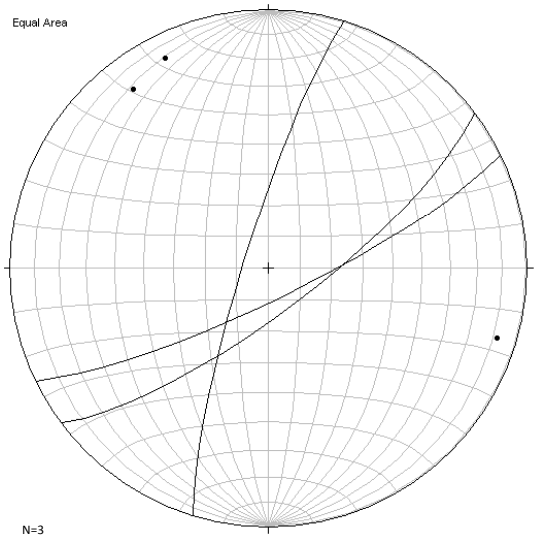

Unclassified Fractures

Appendix A:

Depth: 570.52-582.20

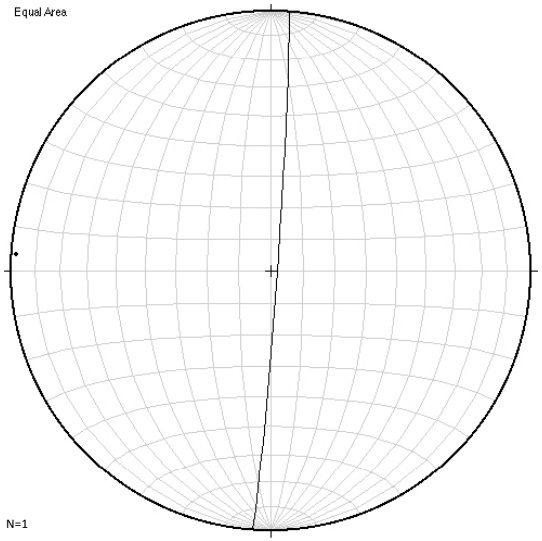

VEINS

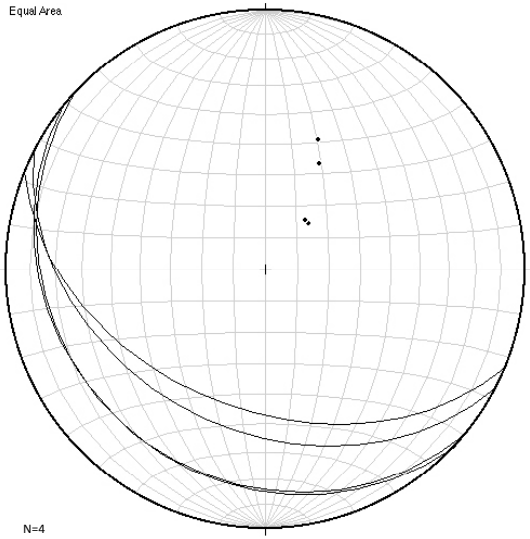

FAULTS

CLASTIC DIKES

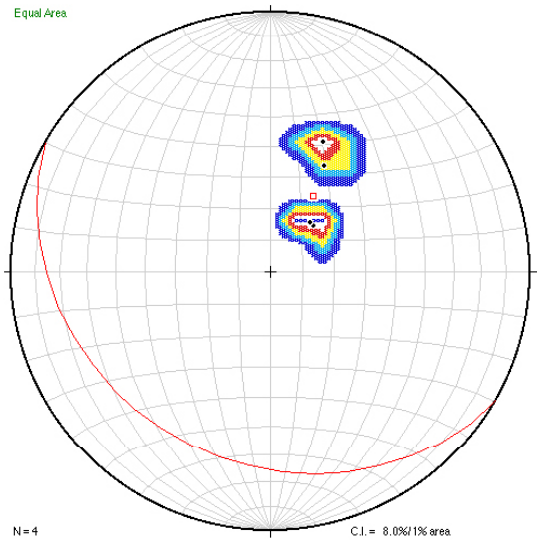

Average Fault Orientation: N60°W, 26°S

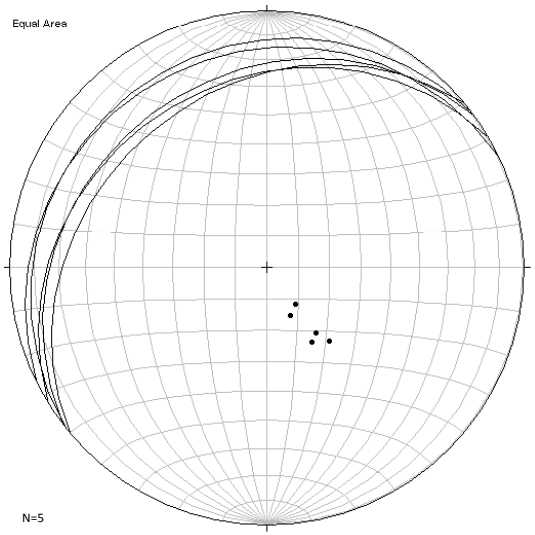

Unclassified Fractures

Appendix A:

Depth: 582.4-587.10

VEINS	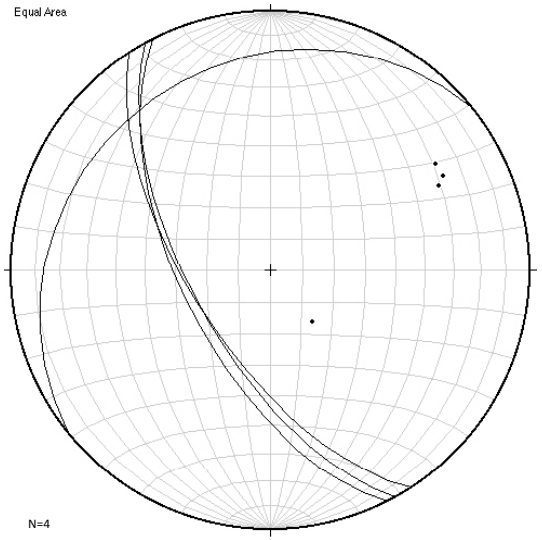 FAULTS	CLASTIC DIKES
	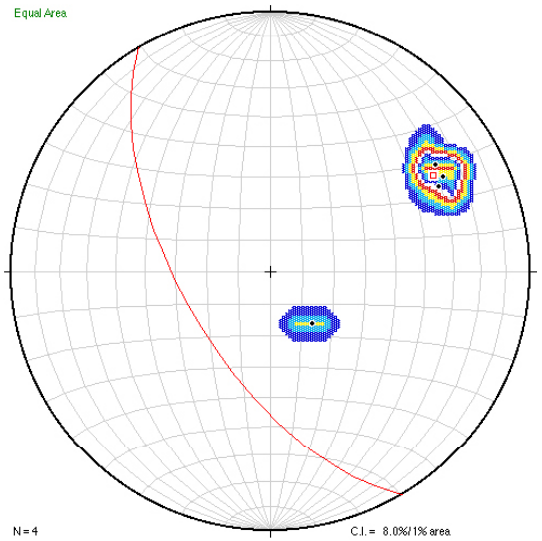 Average Fault Orientation: N30°W, 62°W	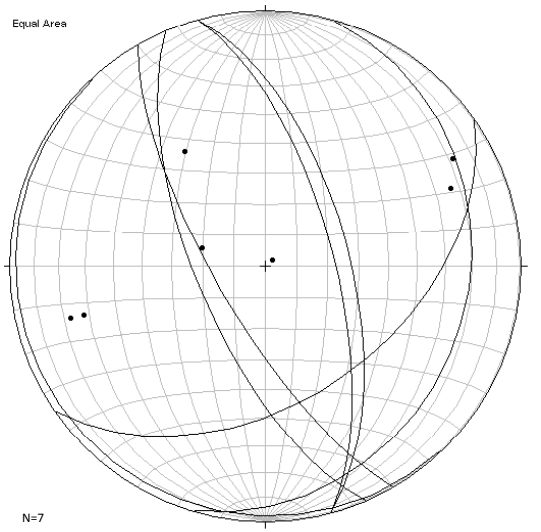 Unclassified Fractures

Appendix A:

Depth: 647.53-666.00

VEINS	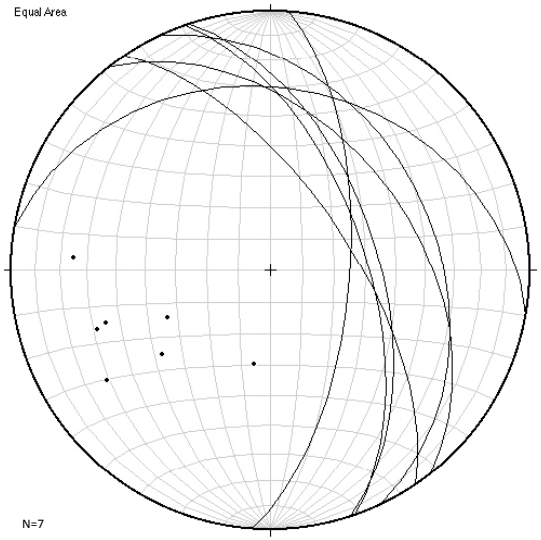 FAULTS	CLASTIC DIKES
	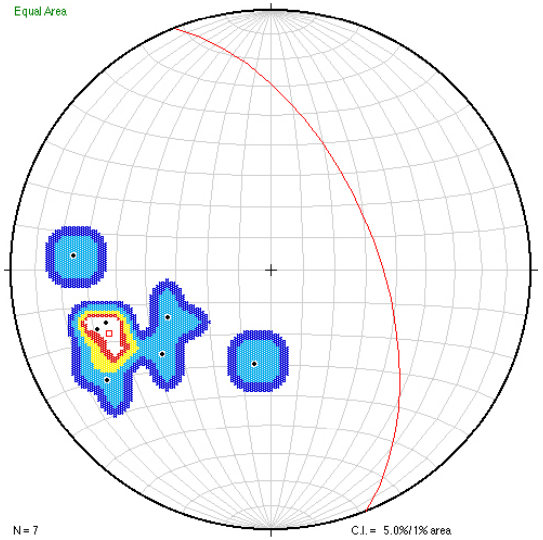 Average Fault Orientation: N22°W, 56°E	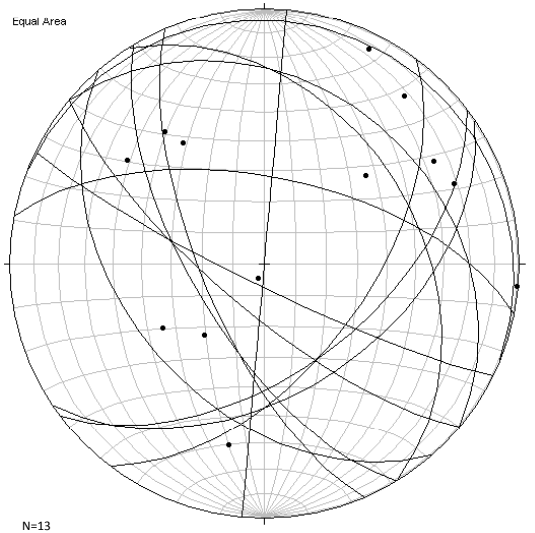 Unclassified Fractures

Appendix A:

Depth: 666.00-701.68

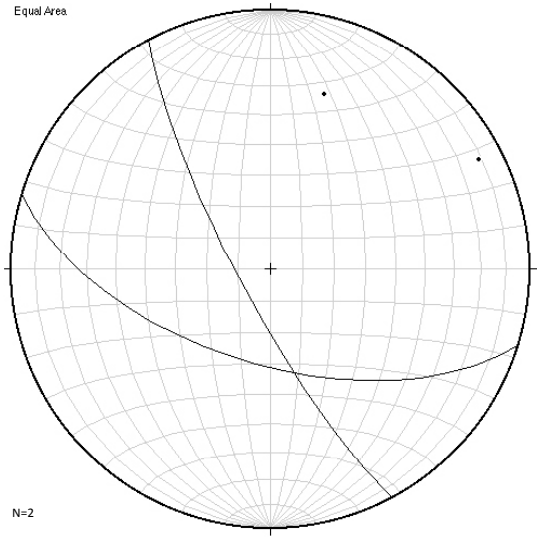

VEINS

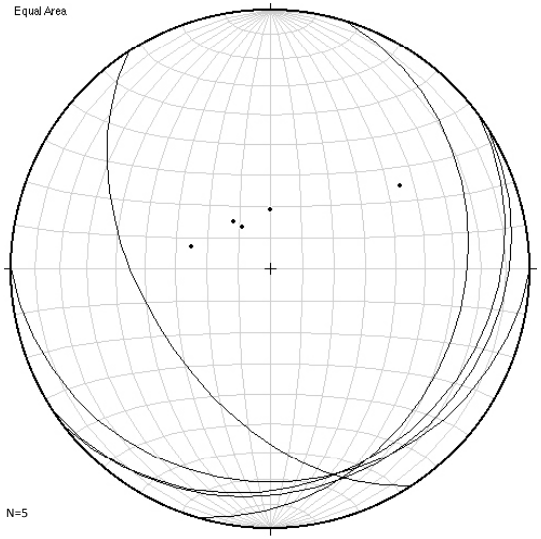

FAULTS

CLASTIC DIKES

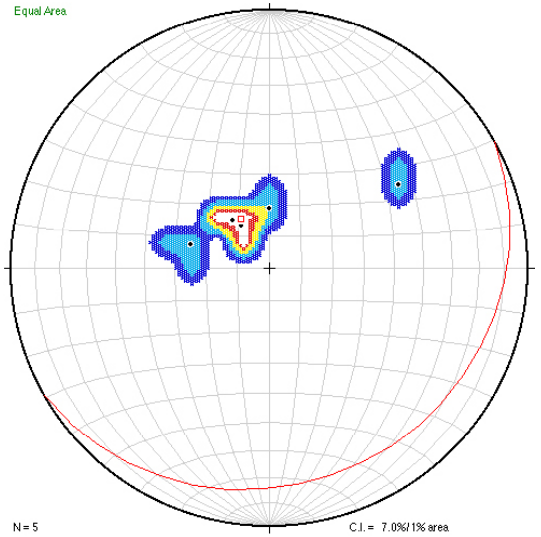

Average Fault Orientation: N61°E, 18°S

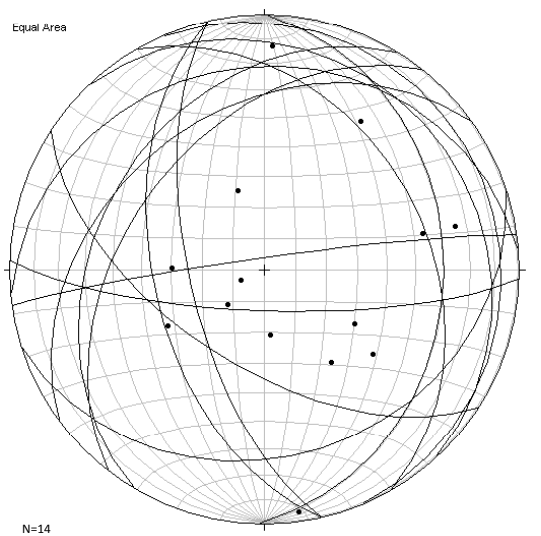

Unclassified Fractures

Appendix A:

Depth: 837.63-852.01

	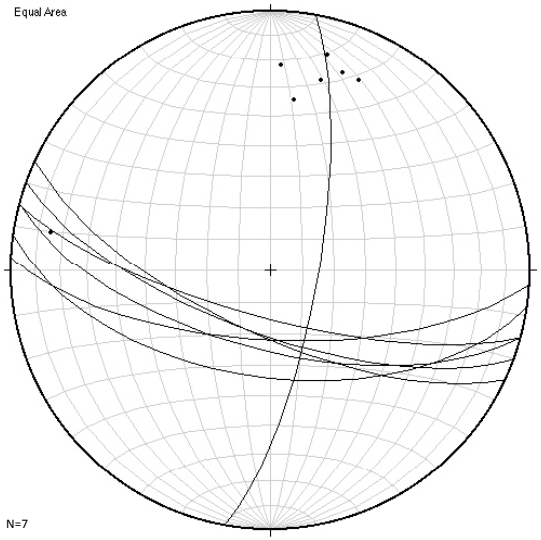	
VEINS	FAULTS	CLASTIC DIKES
	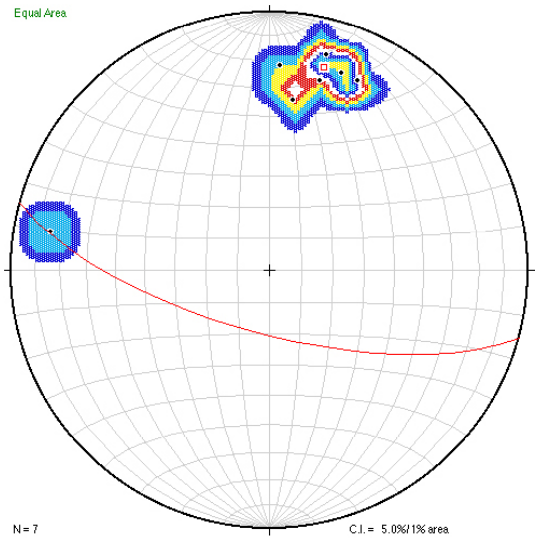	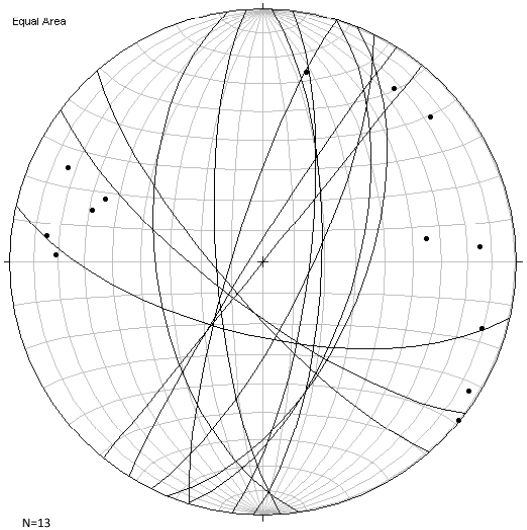
	Average Fault Orientation: N75°W, 70°S	Unclassified Fractures

Appendix A:

Depth: 852.01-875.60

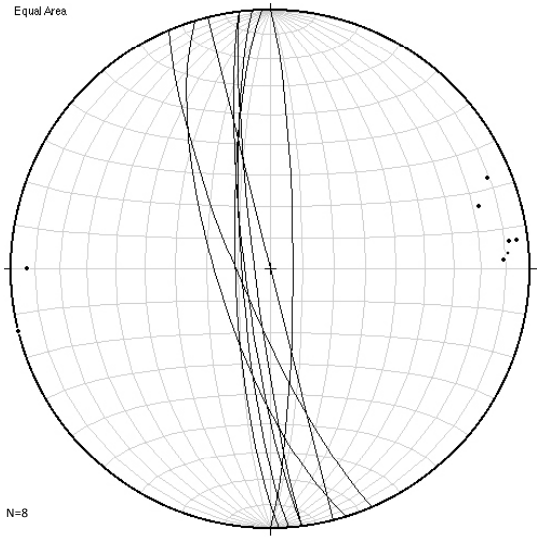

VEINS

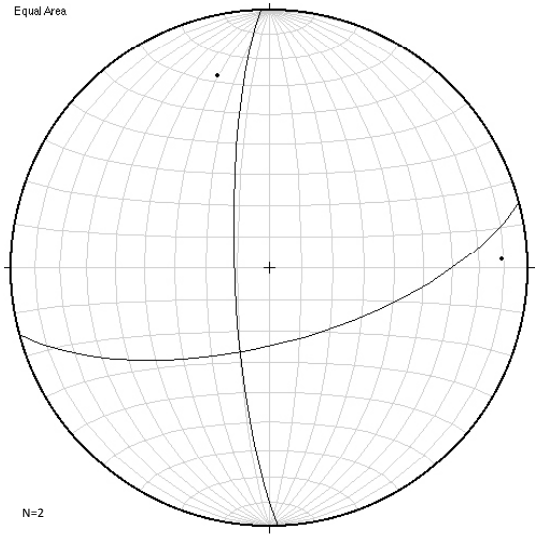

FAULTS

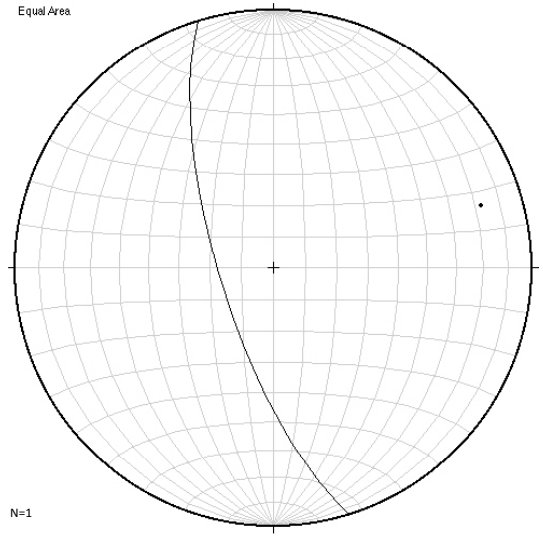

CLASTIC DIKES

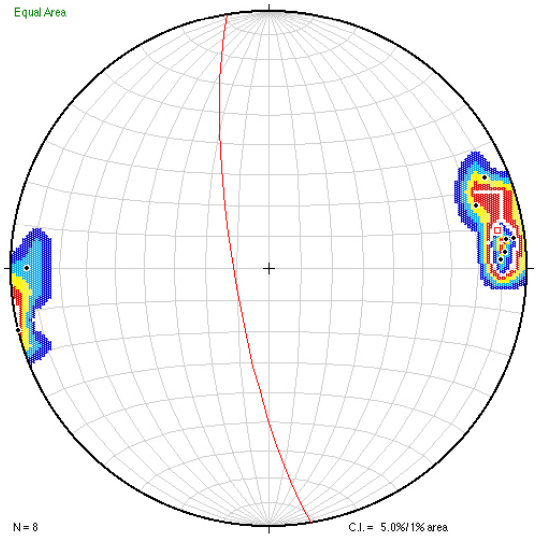

Average Vein Orientation: N9°W, 79°W

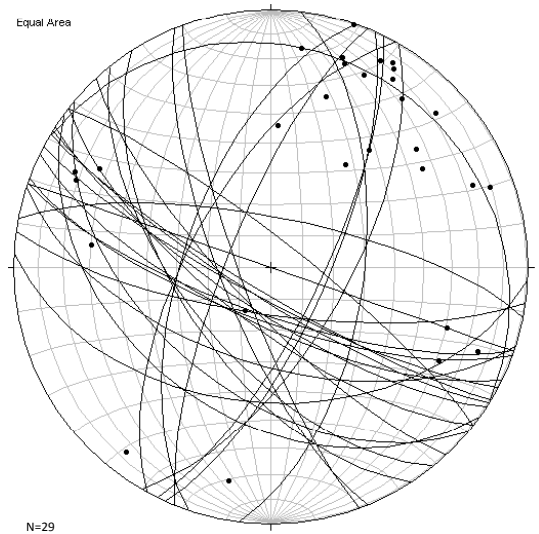

Unclassified Fractures

Appendix A:

Depth: 880.98-886.37

VEINS	FAULTS	CLASTIC DIKES
		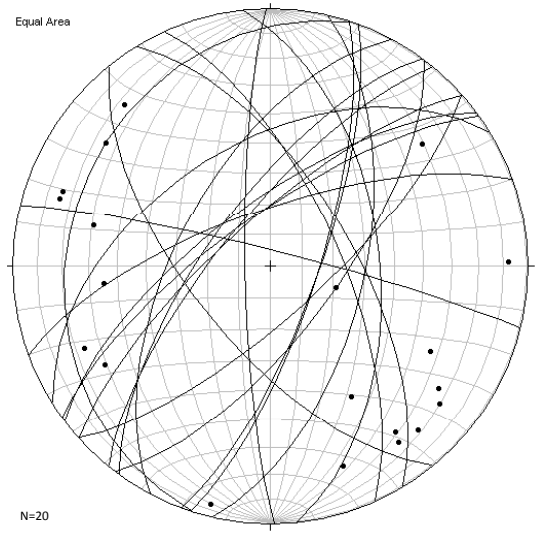 Unclassified Fractures

Appendix A:

Depth: 895.43-897.44

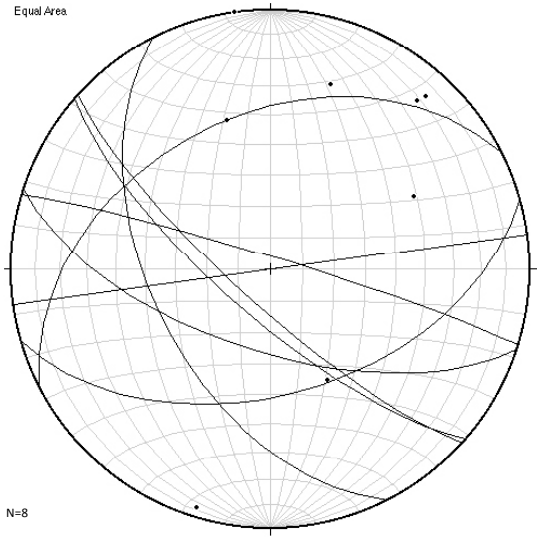

VEINS

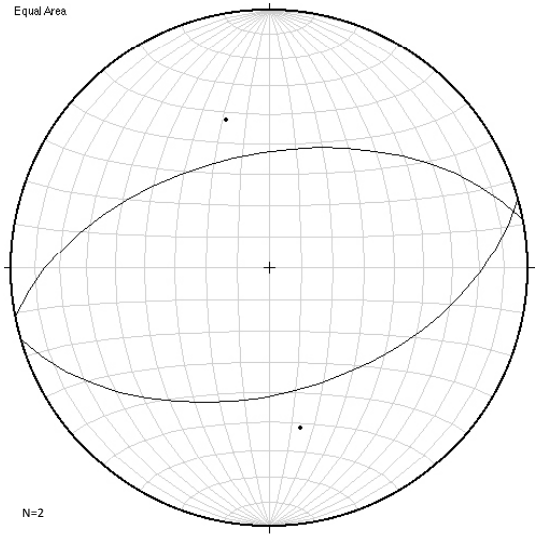

FAULTS

CLASTIC DIKES

Unclassified Fractures

Appendix A:

Depth: 898.11-916.16

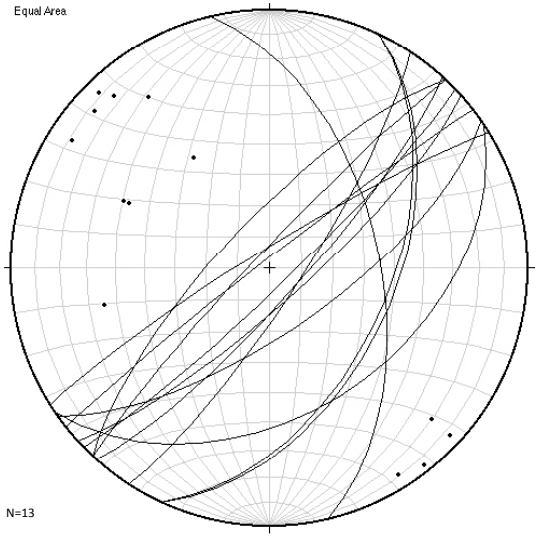

VEINS

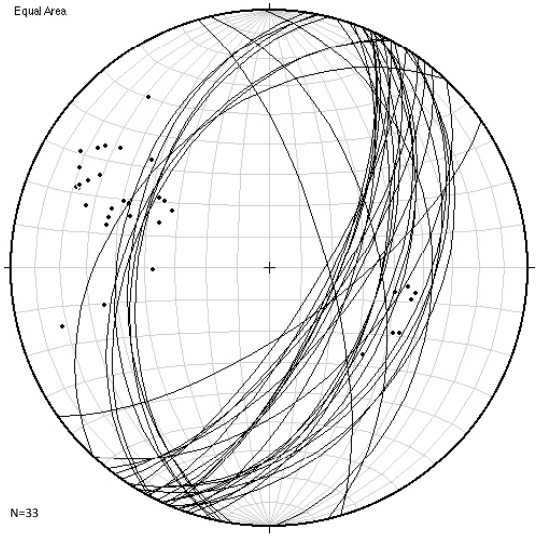

FAULTS

CLASTIC DIKES

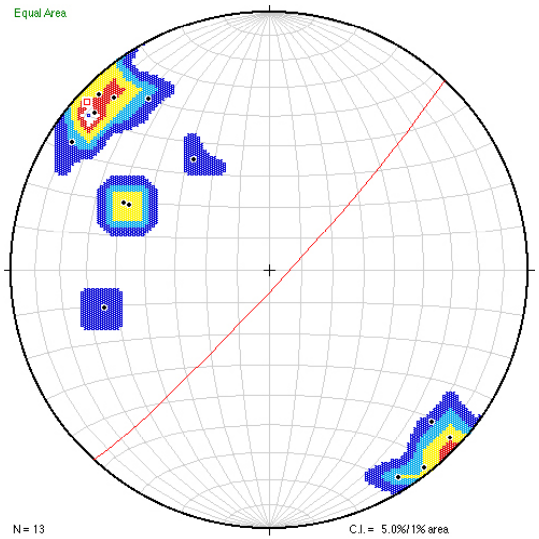

Average Vein Orientation: N43°E, 85°E

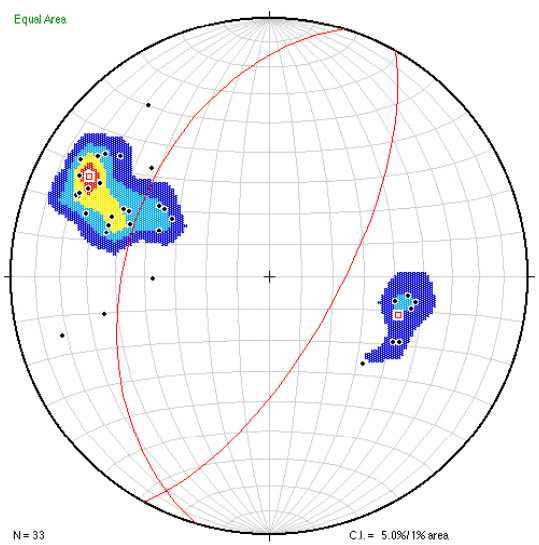

Average Fault Orientations: N29°E, 69°E
N17°E, 43°W

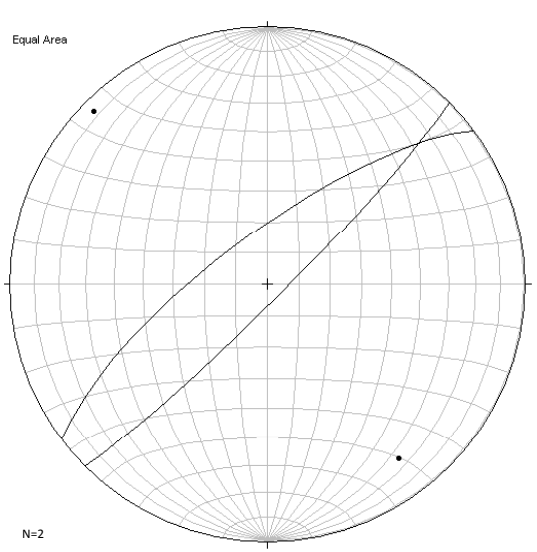

Unclassified Fractures

Appendix A:

Depth: 916.16-926.32

VEINS	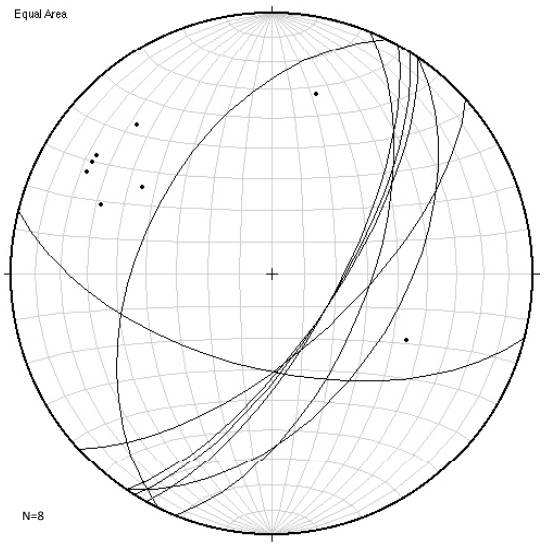 FAULTS	CLASTIC DIKES
	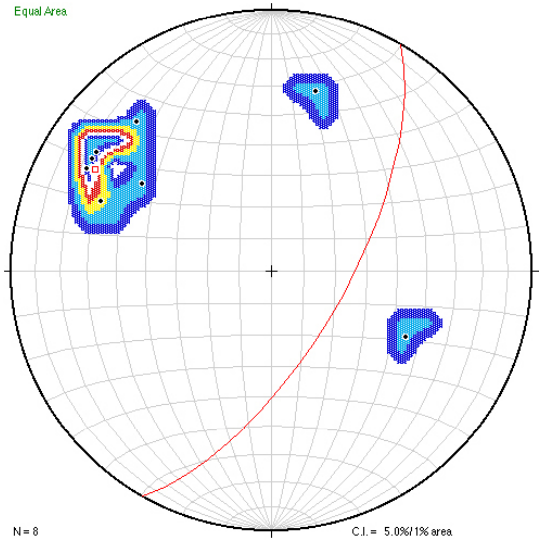 Average Fault Orientation: N30°E, 67°E	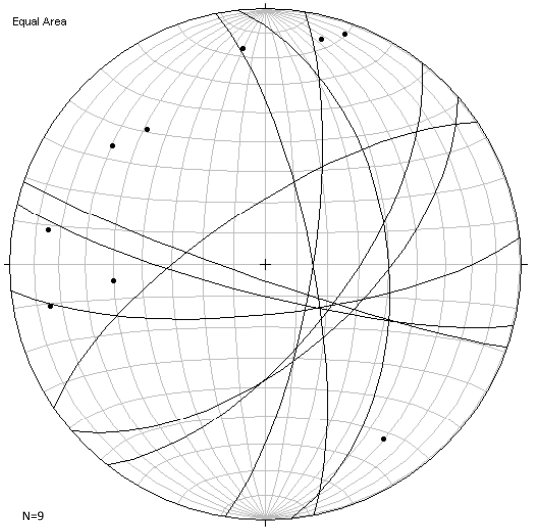 Unclassified Fractures

Appendix A:

Depth: 926.32-971.72

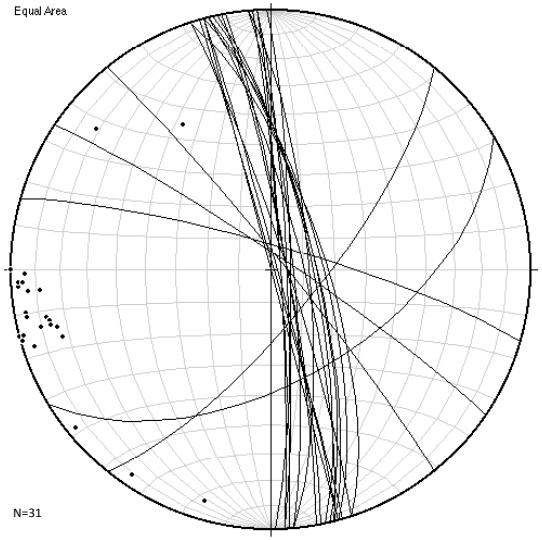

VEINS

FAULTS

CLASTIC DIKES

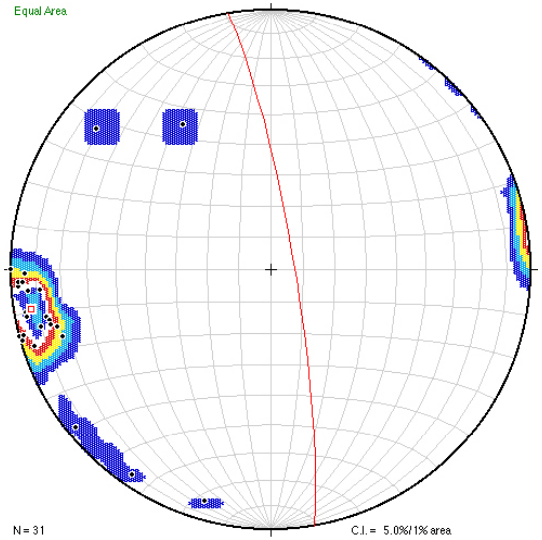

Average Vein Orientation: N9°W, 83°E

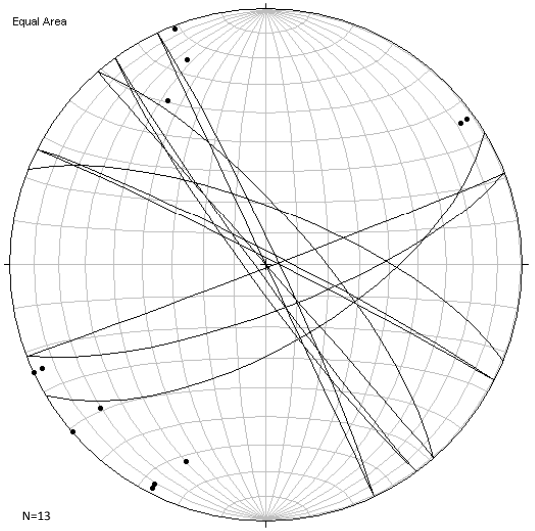

Unclassified Fractures

Appendix A:

Depth: 971.72-1001.94

VEINS	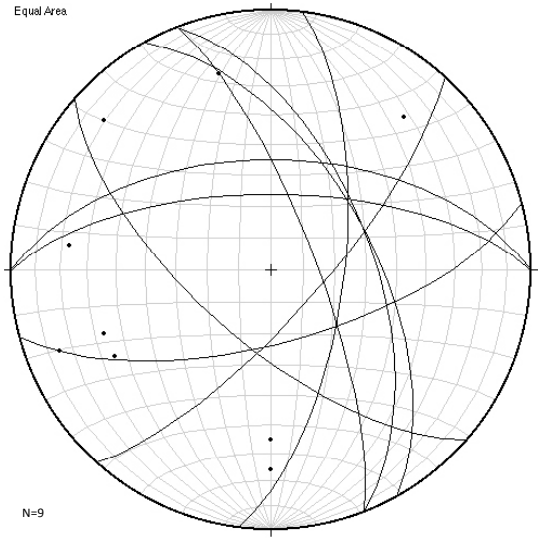 FAULTS	CLASTIC DIKES
		Unclassified Fractures

Appendix A:

Depth: 1036.80-1049.13

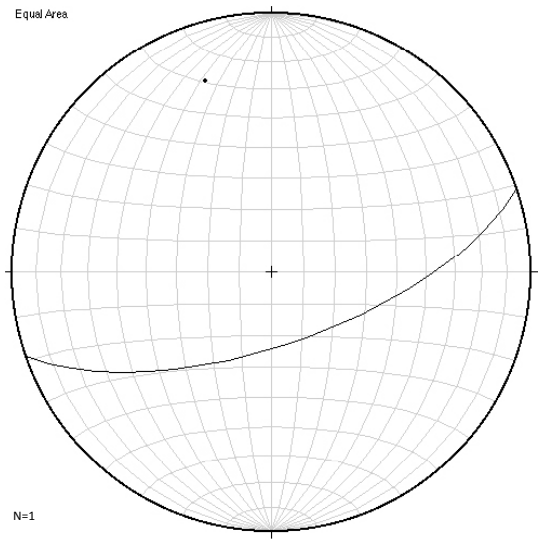

VEINS

FAULTS

CLASTIC DIKES

Unclassified Fractures

Appendix A:

Depth: 1068.84-1082.92

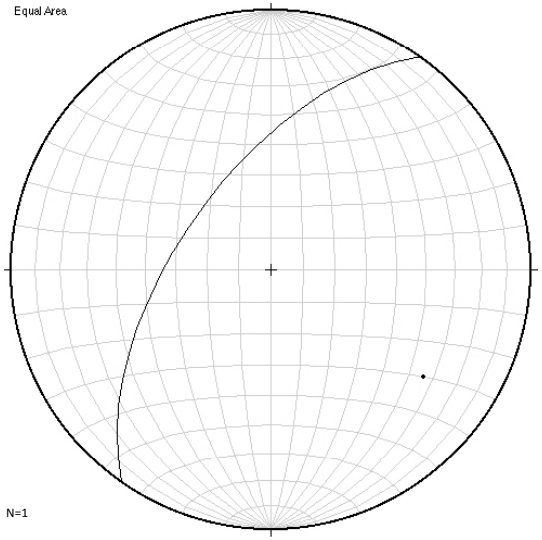

VEINS

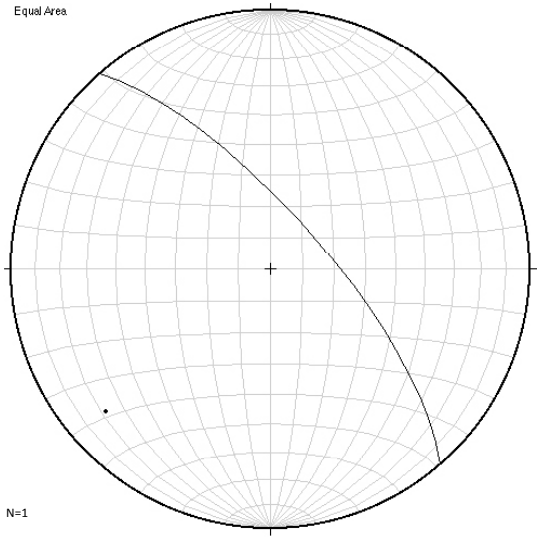

FAULTS

CLASTIC DIKES

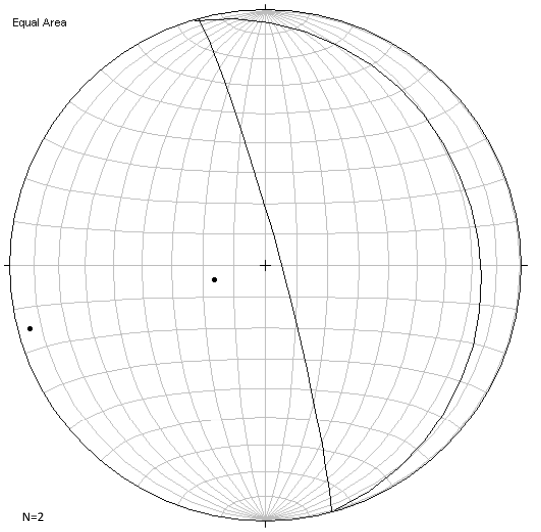

Unclassified Fractures

Appendix A:

Depth: 1100.29-1117.17

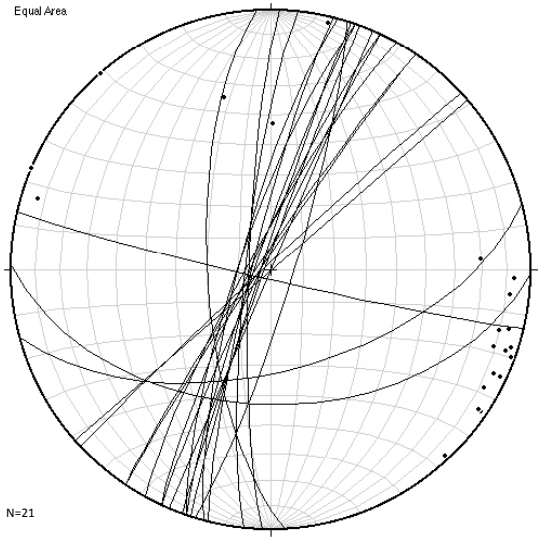

VEINS

FAULTS

CLASTIC DIKES

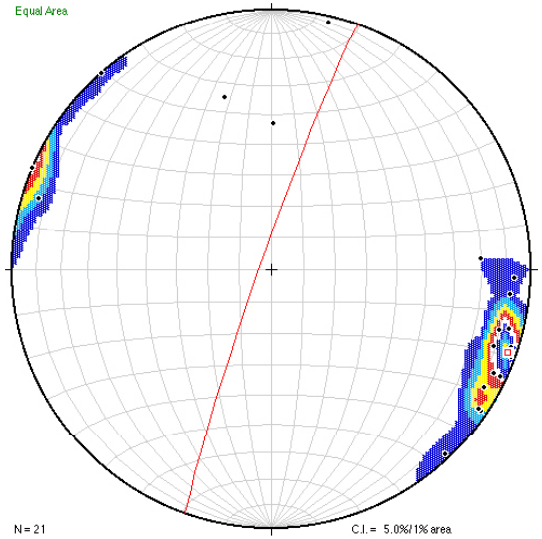

Average Vein Orientation: N20°E, 86°W

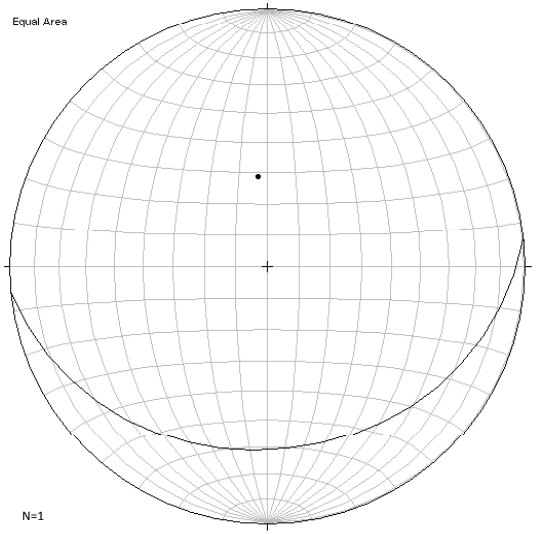

Unclassified Fractures

Appendix B:

398.05-407.24	VEINS			FAULTS			CLASTIC DIKES	
	DIP	DD		DIP	DD		DIP	DD
							35	342
407.61-425.70	**VEINS**			**FAULTS**			**CLASTIC DIKES**	
	DIP	DD		DIP	DD		DIP	DD
				65	198			
				35	124			
				55	216			
				75	288			
				67	144			
				34	262			
497.26-527.41	**VEINS**			**FAULTS**			**CLASTIC DIKES**	
	DIP	DD		DIP	DD		DIP	DD
				77	340			
				70	345			
				85	334			
527.41-546.35	**VEINS**			**FAULTS**			**CLASTIC DIKES**	
	DIP	DD		DIP	DD		DIP	DD
	81	337						
	87	191						
	82	191						
	82	191						
570.52-582.20	**VEINS**			**FAULTS**			**CLASTIC DIKES**	
	DIP	DD		DIP	DD		DIP	DD
	88	94		20	223			
				20	219			
				38	207			
				45	202			
582.40-587.10	**VEINS**			**FAULTS**			**CLASTIC DIKES**	
	DIP	DD		DIP	DD		DIP	DD
				21	321			
				65	237			
				65	241			
				62	243			
647.53-666.00	**VEINS**			**FAULTS**			**CLASTIC DIKES**	
	DIP	DD		DIP	DD		DIP	DD
				65	56			
				65	94			
				30	10			
				44	52			
				36	65			
				60	71			
				56	72			
666.00-701.68	**VEINS**			**FAULTS**			**CLASTIC DIKES**	
	DIP	DD		DIP	DD		DIP	DD
	80	242		26	107			
	60	197		19	143			
				16	147			
				19	180			
				50	237			

837.63-852.01	VEINS			FAULTS			CLASTIC DIKES	
	DIP	DD		DIP	DD		DIP	DD
				75	100			
				70	205			
				75	195			
				70	200			
				65	195			
				68	183			
				56	188			
852.01-875.60	**VEINS**			**FAULTS**			**CLASTIC DIKES**	
	DIP	DD		DIP	DD		DIP	DD
	79	268		79	268		73	253
	80	247		66	165			
	83	90						
	90	76						
	73	253						
	85	263						
	81	266						
	82	263						
895.43-897.44	**VEINS**			**FAULTS**			**CLASTIC DIKES**	
	DIP	DD		DIP	DD		DIP	DD
	50	164		50	164			
	86	17		53	349			
	64	198						
	79	222						
	40	333						
	75	221						
	90	172						
	52	243						

Appendix B:

898.11-916.16	VEINS		FAULTS		CLASTIC DIKES	
	DIP	DD	DIP	DD	DIP	DD
	87	322	70	145		
	70	145	55	77		
	55	77	50	115		
	50	115	52	115		
	52	115	69	113		
	84	136	37	89		
	80	132	72	74		
	84	328	70	113		
	43	146	69	114		
	79	138	67	116		
	80	123	48	280		
	75	313	41	281		
	85	313	47	283		
			45	278		
			47	297		
			45	298		
			41	313		
			68	127		
			63	129		
			52	133		
			36	121		
			55	111		
			72	118		
			55	105		
			55	108		
			38	113		
			40	123		
			42	123		
			48	111		
			75	122		
			70	125		
			64	119		
			64	109		

916.16-926.32	VEINS		FAULTS		CLASTIC DIKES	
	DIP	DD	DIP	DD	DIP	DD
			60	112		
			48	296		
			50	124		
			70	122		
			66	138		
			60	194		
			70	119		
			70	124		

926.32-971.72	VEINS		FAULTS		CLASTIC DIKES	
	DIP	DD	DIP	DD	DIP	DD
	73	432				
	87	446				
	87	447				
	85	447				
	78	445				
	77	438				
	76	437				
	76	436				
	80	436				
	85	440				
	83	445				
	85	72				
	85	72				
	55	149				
	55	149				
	85	34				
	85	34				
	85	79				
	85	79				
	75	129				
	75	129				
	90	435				
	90	450				
	82	16				
	82	16				
	86	51				
	86	51				
	88	75				
	74	75				
	89	434				
	84	449				

971.72-1001.94	VEINS		FAULTS		CLASTIC DIKES	
	DIP	DD	DIP	DD	DIP	DD
			58	69		
			75	132		
			67	165		
			67	221		
			67	97		
			58	61		
			76	69		
			55	360		
			66	360		

1036.80-1049.13	VEINS		FAULTS		CLASTIC DIKES	
	DIP	DD	DIP	DD	DIP	DD
	67	161				

1068.84-1082.92	VEINS		FAULTS		CLASTIC DIKES	
	DIP	DD	DIP	DD	DIP	DD
	61	305	73	49		

Appendix B:

1100.29-1117.17	VEINS			FAULTS			CLASTIC DIKES	
	DIP	DD		DIP	DD		DIP	DD
	83	107						
	88	290						
	87	295						
	88	317						
	83	272						
	82	276						
	85	289						
	87	304						
	86	304						
	90	113						
	87	193						
	87	288						
	80	285						
	80	289						
	84	284						
	83	299						
	90	139						
	70	267						
	58	165						
	47	181						
	84	295						